the plant journal

SEB SOCIETY FOR EXPERIMENTAL BIOLOGY

The Plant Journal (2022) doi: 10.1111/tpj.15747

Cavity surface residues of PAD4 and SAG101 contribute to EDS1 dimer signaling specificity in plant immunity

Joram A. Dongus[1,2], Deepak D. Bhandari[1,3], Eva Penner[1], Dmitry Lapin[1,4], Sara C. Stolze[5], Anne Harzen[5], Monika Patel[6], Lani Archer[6], Lucas Dijkgraaf[1,4], Jyoti Shah[6], Hirofumi Nakagami[5] and Jane E. Parker[1,7,*]

[1]*Department of Plant-Microbe Interactions, Max Planck Institute for Plant Breeding Research, Carl-von-Linné-Weg 10, 50829, Cologne, Germany,*

[2]*Laboratory of Plant Physiology, Wageningen University, Droevendaalsesteeg 1, 6700, AA Wageningen, The Netherlands,*

[3]*Plant Research Laboratory, Michigan State University, 612, Wilson Road, East Lansing, Michigan 48824, USA,*

[4]*Plant-Microbe Interactions, Utrecht University, Padualaan 8, 3584, CH Utrecht, The Netherlands,*

[5]*Protein Mass Spectrometry, Max Planck Institute for Plant Breeding Research, Carl-von-Linné-Weg 10, 50829, Cologne, Germany,*

[6]*Department of Biological Sciences and BioDiscovery Institute, University of North Texas, 1511 West Sycamore, Denton, 76201, Texas, USA, and*

[7]*Cologne-Düsseldorf Cluster of Excellence on Plant Sciences (CEPLAS), 40225, Düsseldorf, Germany*

Received 27 October 2021; revised 9 March 2022; accepted 17 March 2022.
*For correspondence (e-mail parker@mpipz.mpg.de).

SUMMARY

Arabidopsis pathogen effector-triggered immunity (ETI) is controlled by a family of three lipase-like proteins (EDS1, PAD4, and SAG101) and two subfamilies of HET-S/LOB-B (HeLo)-domain "helper" nucleotide-binding/leucine-rich repeats (ADR1s and NRG1s). EDS1-PAD4 dimers cooperate with ADR1s, and EDS1-SAG101 dimers with NRG1s, in two separate defense-promoting modules. EDS1-PAD4-ADR1 and EDS1-SAG101-NRG1 complexes were detected in immune-activated leaf extracts but the molecular determinants for specific complex formation and function remain unknown. EDS1 signaling is mediated by a C-terminal EP domain (EPD) surface surrounding a cavity formed by the heterodimer. Here we investigated whether the EPDs of PAD4 and SAG101 contribute to EDS1 dimer functions. Using a structure-guided approach, we undertook a comprehensive mutational analysis of Arabidopsis PAD4. We identify two conserved residues (Arg314 and Lys380) lining the PAD4 EPD cavity that are essential for EDS1-PAD4–mediated pathogen resistance, but are dispensable for the PAD4-mediated restriction of green peach aphid infestation. Positionally equivalent Met304 and Arg373 at the SAG101 EPD cavity are required for EDS1-SAG101 promotion of ETI-related cell death. In a PAD4 and SAG101 interactome analysis of ETI-activated tissues, PAD4^{R314A} and SAG101^{M304R} EPD variants maintain interaction with EDS1 but lose association, respectively, with helper nucleotide-binding/leucine-rich repeats ADR1-L1 and NRG1.1, and other immune-related proteins. Our data reveal a fundamental contribution of similar but non-identical PAD4 and SAG101 EPD surfaces to specific EDS1 dimer protein interactions and pathogen immunity.

Keywords: NLR, EDS1, PAD4, SAG101, ETI, immunity, plant.

INTRODUCTION

Plants deploy innate immunity receptor barriers against pathogen infection. Pattern recognition receptors (PRRs) at the plasma membrane detect microbial or modified host molecules to activate pattern-triggered immunity (PTI) (Albert et al., 2020; Couto & Zipfel, 2016; Wan, Frohlich, et al., 2019). Intracellular nucleotide-binding/leucine-rich repeat (NLR) receptors recognize pathogen-secreted virulence factors called effectors, which disable or modulate PTI (Cui et al., 2015; Monteiro & Nishimura, 2018). In an effector-triggered immune (ETI) response, NLR-effector recognition amplifies generally weaker PTI defenses. This culminates in strong resistance and localized host cell death (Cui et al., 2015; Yuan et al., 2020). NLRs fall into three major subgroups categorized by their N-terminal signaling domains: (i) a Toll/interleukin-1 receptor (TIR) domain in TIR-type NLRs (TNLs), (ii) a coiled-coil (CC) domain in CC-type NLRs (CNLs), and (iii) an RPW8-like CC_R

(HET-S/LOB-B [HeLo]) domain in CC_R-type NLRs (RNLs) (Feehan et al., 2020; Lapin et al., 2022; Monteiro & Nishimura, 2018; Ngou et al., 2021). Pathogen-sensing NLR receptors engage a network of related and unrelated NLRs, called helper NLRs, including the RNLs, to promote ETI (Feehan et al., 2020; Wroblewski et al., 2018; Wu et al., 2017; Zhang et al., 2019). Besides PTI and ETI, a host basal immunity response slows infection by virulent pathogens, and is likely the combined outcome of residual PTI (after effector interference) and weak ETI (Dongus & Parker, 2021; Jones & Dangl, 2006).

Three Enhanced Disease Susceptibility 1 (EDS1) family proteins, EDS1 itself, Phytoalexin-Deficient 4 (PAD4) and Senescence-Associated Gene 101 (SAG101) are important regulators of ETI and basal immunity (Dongus & Parker, 2021; Lapin et al., 2020). They are characterized by the fusion of an N-terminal lipase-like domain (LLD) and a unique C-terminal α-helical bundle domain, referred to as the EP-domain (EPD) (PFAM database: PF18117; (Dongus & Parker, 2021, Lapin et al., 2020, Voss et al., 2019, Wagner et al., 2013, Wiermer et al., 2005). EDS1 forms exclusive heterodimers with PAD4 or SAG101, which appear to be the minimal functional units for conferring pathogen immunity (Bhandari et al., 2019; Gantner et al., 2019; Ke et al., 2019; Lapin et al., 2019; Neubauer et al., 2020; Pruitt et al., 2021; Rietz et al., 2011; Voss et al., 2019; Wagner et al., 2013). EDS1 and PAD4, but not SAG101, harbor a conserved catalytic Ser-Asp-His (S-D-H) triad in the LLD, a quintessential feature of α/β-hydrolase proteins (Mindrebo et al., 2016). However, these residues are dispensable for pathogen basal immunity and ETI in *Arabidopsis thaliana* (*At*; Arabidopsis), suggesting that EDS1 and PAD4 are pseudoenzymes (Louis et al., 2012; Voss et al., 2019; Wagner et al., 2013). Notably, *At*PAD4 requires the catalytic triad S-D, but not H residue, to limit proliferation of the leaf-sucking insect green peach aphid (GPA) (Dongus et al., 2020; Louis et al., 2012; Louis & Shah, 2015). While the PAD4 EPD is essential for activating immune responses against oomycete and bacterial pathogens, PAD4 alone confers GPA resistance without its EPD or *EDS1* and *SAG101* (Dongus et al., 2020; Pegadaraju et al., 2007), highlighting a distinctive Arabidopsis PAD4 LLD activity in biotic stress signaling.

In Arabidopsis, two genetically separate EDS1 signaling modules recruit different RNL subfamilies, Activated Disease Resistance 1s (ADR1s) and N Requirement Gene 1s (NRG1s), for immunity signaling. The first module, consisting of EDS1, SAG101, and genetically redundant RNLs NRG1.1 and NRG1.2, is engaged by TNL receptors to mediate host cell death and pathogen resistance (Castel, Ngou, et al., 2019; Lapin et al., 2019; Saile et al., 2020; Sun et al., 2021; Wu et al., 2019). The EDS1-SAG101 dimer associates with NRG1 family members after TNL activation, suggesting these components signal as a TNL-induced protein complex (Sun et al., 2021). The second module, consisting of EDS1-PAD4 with genetically redundant ADR1 family RNLs ADR1, ADR1-L1, and ADR1-L2, also forms a complex in immunity-induced tissues (Lapin et al., 2019; Sun et al., 2021; Wu et al., 2019; Wu, Tian, Liu, Zhang, & Li, 2021). Genetic studies showed that the EDS1-PAD4-ADR1 module is responsible for basal immunity, which contributes to varied extents to TNL and CNL ETI (Dongus & Parker, 2021; Pruitt et al., 2021; Saile et al., 2020; Sun et al., 2021; Wu et al., 2019). In TNL ETI to *Pseudomonas syringae* bacteria, this EDS1-PAD4 controlled module enables rapid transcriptional mobilization of immune receptor and defense genes. This module also reprograms the phytohormone network to boost salicylic acid (SA) resistance and dampen SA-antagonizing jasmonic acid pathways (Bhandari et al., 2019; Bonardi et al., 2011; Castel, Ngou, et al., 2019; Cui et al., 2017; Cui et al., 2018; Mine et al., 2017; Saile et al., 2020). Recent evidence links Arabidopsis EDS1-PAD4 and ADR1s to PTI conferred by cell surface receptor-like kinases (RLKs) and receptor-like proteins (RLPs) (Pruitt et al., 2021; Tian et al., 2021). Pathogen immunity, triggered by RLP23 and its co-receptor SOBIR recognizing an oomycete PAMP (nlp20), relies strongly on the EDS1-PAD4 dimer and ADR1s, but much less on SAG101 or NRG1s (Pruitt et al., 2021, Tian et al., 2021). Pools of EDS1, PAD4, and ADR1 proteins were detected in close proximity to SOBIR1, implicating the EDS1-PAD4-ADR1 module as an integrator of immune signals initiated at the plasma membrane (Pruitt et al., 2021).

Functional analyses of an *At*EDS1-*At*SAG101 dimer crystal structure and derived *At*EDS1-*At*PAD4 or tomato EDS1-SAG101 structural models showed that juxtaposed partner N-terminal LLDs drive dimerization via an EDS1 hydrophobic helix (αH) fitting into similar hydrophobic grooves of PAD4 or SAG101 (Gantner et al., 2019; Voss et al., 2019; Wagner et al., 2013). Dimerization of both EDS1-PAD4 and EDS1-SAG101 creates a C-terminal EPD cavity (Voss et al., 2019; Wagner et al., 2013). Further mutational analysis identified several *At*EDS1 residues lining the EPD cavity, of which most are positively charged, and are necessary for pathogen immunity and for induced EDS1-SAG101 association with *At*NRG1.1 (Bhandari et al., 2019; Gantner et al., 2019; Lapin et al., 2019; Sun et al., 2021; Wagner et al., 2013). These data suggest that the EDS1 dimer EPD cavity, directly or indirectly, confers association with RNLs. Our aim here was to explore whether the EPD surfaces of PAD4 and SAG101 contribute to EDS1 dimer recruitment of specific RNL sub-types. We identify Arabidopsis PAD4 and SAG101 EPD residues at the cavity surface that are indispensable for EDS1 heterodimer-mediated pathogen immunity, but not for PAD4-dependent GPA resistance. A comparative PAD4 and SAG101 interactome analysis in TNL-activated tissues shows that PAD4 EPD

residue Arg314 and SAG101 Met304 contribute to EDS1 dimer binding of respective helper NLRs, ADR1-L1 and NRG1.1. An intact EDS1-PAD4 dimer EPD signaling surface also promotes its association with RPW8-like CC_R protein, HR4.

RESULTS

Arabidopsis PAD4 EPD cavity residues Arg314 and Lys380 are required for EDS1-PAD4 immunity

Several EDS1 EPD cavity surface residues control timely defense reprogramming and pathogen immunity (Bhandari et al., 2019; Gantner et al., 2019; Lapin et al., 2019, 2020). We surveyed *At*PAD4 EPD helices and selected amino acids that are conserved in Angiosperm lineages and are surface-exposed in an EDS1-PAD4 structural model (Figure S1a–e; Video S1). The amino acids were mutated to alanine, and we transformed corresponding *At*PAD4 variants in a *pPAD4:StrepII-YFP-cPAD4* (PAD4 cDNA) vector backbone (Dongus et al., 2020) into an Arabidopsis *pad4-1/sag101-3* mutant. Independent T1 generation *PAD4* stable transgenic lines were tested for complementation of *pad4–/sag101-3* disease susceptibility by inoculating plants with TNL (Recognition of *Peronospora parasitica* 4, RPP4) recognizing *Hyaloperonospora arabidopsidis* (*Hpa*) isolate EMWA1. All *AtPAD4* variant lines exhibited an ETI response similar to wild-type (WT) Columbia-0 (Col-0) except lines expressing *At*PAD4^{R314A} and *At*PAD4^{K380A}, which were as susceptible as *pad4-1/sag101-3*, (Figure 1a; Figure S1f; Video S1). As shown in Figure 1a, Figure S2a, and Video S1, Arg314 (R314) and Lys380 (K380) of PAD4 are close to but do not directly contact EDS1 EPD residues in the heterodimer structure (Wagner et al., 2013). The YFP-tagged *At*PAD4^{R314A} and *At*PAD4^{K380A} proteins interacted with *At*EDS1 in *Nicotiana benthamiana* (*Nb*; *Nb* tobacco) transient expression and immunoprecipitation (IP) assays, although they accumulated less well than WT PAD4-YFP, particularly PAD4^{K380A} (Figure S2b). We concluded that these PAD4 EPD mutations disrupt TNL ETI signaling but not dimer formation with EDS1.

We selected two independent homozygous transgenic lines for *At*PAD4^{WT}, *At*PAD4^{R314A}, and *At*PAD4^{K380A}, and quantified immune outputs. We first measured their TNL (RPP4) ETI responses to *Hpa* EMWA1, TNL (Resistance to *Ralstonia solancearum 1*-Resistant *to Pseudomonas syringae 4*, RRS1-RPS4) ETI responses to *Pseudomonas syringae* pv. *tomato* DC3000 (*Pst)* expressing avrRps4 (*Pst avrRps4*), and basal immunity to virulent *Pst* DC3000 (Figure 1b–d). *At*PAD4^{R314A} and *At*PAD4^{K380A} lines were as susceptible as *pad4-1/sag101-3* in all pathogen assays, while Col-0 and *At*PAD4^{WT} transgenic lines were resistant (Figure 1b–d). We observed similar pathogen infection phenotypes in stable transgenic lines expressing corresponding genomic YFP-PAD4 forms in *pad4-1/sag101-3* (denoted gPAD4^{WT}, gPAD4^{R314A}, and gPAD4^{K380A}) (Figure S3a–c). These gPAD4 transgenic lines had generally higher PAD4 protein levels than lines expressing cPAD4 forms (Figure S3d) (Bhandari et al., 2019). Indeed, the signaling defective gPAD4^{R314A} and gPAD4^{K380A} lines accumulated similar protein amounts as complementing cPAD4^{WT} lines (Figure S3d). These data suggest that reduced protein levels of PAD4^{R314A} and PAD4^{K380A} do not explain their TNL immunity defects. All Arabidopsis *At*PAD4 and *At*gPAD4 WT and mutant variant lines displayed a PAD4 nucleocytoplasmic localization (Figure S4), suggesting that the EPD mutations do not influence PAD4 subcellular localization. We concluded that *At*PAD4 EPD cavity surface residues R314 and K380 are important for EDS1-PAD4 controlled TNL ETI and basal immunity.

An essential *At*EDS1 EPD residue R493 can be functionally replaced by a positively charged lysine (*At*EDS1^{R493K}) (Bhandari et al., 2019). By contrast, exchanging R314 or K380 of *At*PAD4 with positive residues (to give *At*PAD4^{R314K} and *At*PAD4^{K380R}) did not complement *pad4-1/sag101-3* in TNL (RPP4) ETI to *Hpa* EMWA1 in independent T1 transgenic lines (Figure S5). This suggests that precise amino acid coordinates are required at these PAD4 EPD cavity sites, rather than a positive charge. For further analysis we used cDNA lines of *At*PAD4^{R314A} and *At*PAD4^{K380A} exchange mutants in *pad4-1/sag101-3*. To assess if *At*PAD4^{R314A} and *At*PAD4^{K380A} retain any residual signaling activity, defense marker gene expression was quantified by quantitative reverse transcription polymerase chain reaction (PCR) in mock- and *Pst avrRps4*-treated leaves at 24 hpi (Bhandari et al., 2019; Cui et al., 2017). In contrast to Col-0 and *At*PAD4^{WT} strong upregulation of genes belonging to SA-dependent (*Isochorismate Synthase 1* [*ICS1*], *avrPphB Susceptible 3* [*PBS3*], and *Pathogenesis-related 1* [*PR1*]) and SA-independent (*Flavin-containing Monooxygenase 1* [*FMO1*]) pathways, the *pad4-1/sag101-3* mutant and the *At*PAD4^{R314A} and *At*PAD4^{K380A} transgenic lines failed to induce defense gene expression (Figure S6). Put together, the data show that PAD4^{R314A} and PAD4^{K380A} are immune signaling-deficient variants of PAD4.

Arabidopsis *PAD4* functions independently of *EDS1* and *SAG101* in resistance to GPA, a phloem sap consuming hemipteran (Pegadaraju et al., 2007). In contrast to PAD4^{R314A} and PAD4^{K380A} disabling TNL-mediated ETI and bacterial basal immunity, these PAD4 mutants limited GPA proliferation to the same extent as Col-0, *eds1-2*, and *At*PAD4^{WT}, while *pad4-1/sag101-3* showed increased GPA fecundity (Figure 1e). This result is in line with the observation that the PAD4 LLD alone, without the EPD, is sufficient for limiting GPA infestation, and that resistance to GPA relies on LLD predicted catalytic triad-located Ser118 (S118) and Asp178 (D178) (Dongus et al., 2020; Louis et al., 2012). These data show that *At*PAD4^{R314A} and

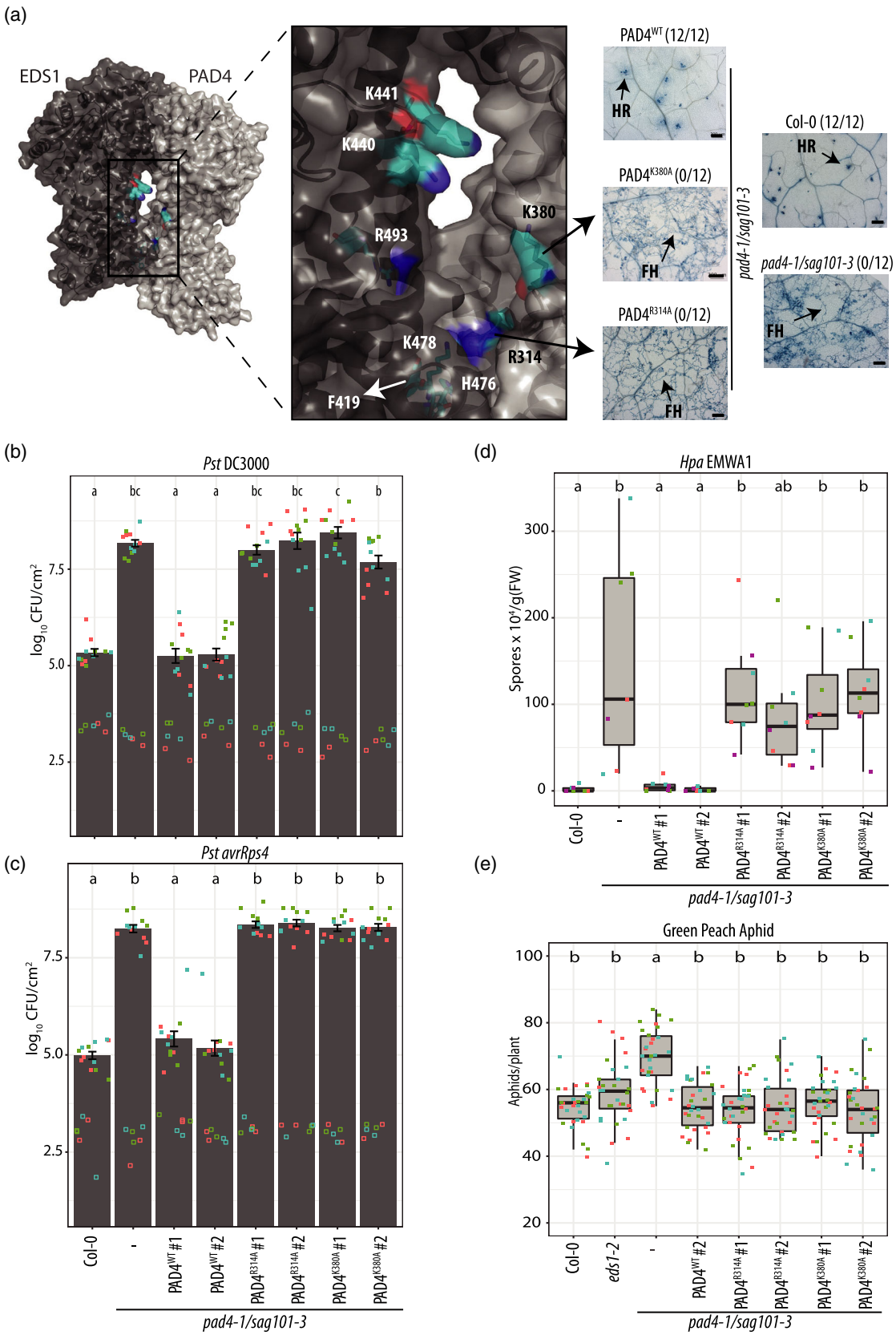

Figure 1. Infection phenotypes of PAD4 EP-domain mutants in Arabidopsis. (a) Arabidopsis EDS1-PAD4 heterodimer model (based on Arabidopsis EDS1-SAG101 crystal structure; PDB (protein data bank): 4NFU; Wagner et al., 2013). EDS1 (black) and PAD4 (gray) with highlighted residues previously mutated in EDS1, and R314 and K380 of *At*PAD4. Highlighted residues display carbon atoms in turquoise, oxygen atoms in red and nitrogen atoms in blue (Bhandari et al., 2019; Lapin et al., 2019). See Video S1 for a three-dimensional representation of Arabidopsis EDS1-PAD4 cavity residues shown in (a). Microscopic immunity phenotypes of 3-week-old Arabidopsis T1 PAD4^{R314A}, T1 PAD4^{K380A}, and T3 PAD4^{WT} at 6 days postinfection (dpi) with *Hpa* isolate EMWA1 (4×10^4 spores per ml; recognized by TNL RPP4). Trypan blue-stained leaves showing free hyphae (FH) and hypersensitive cell death (hypersensitive response, HR). Col-0 (resistant) and *pad4-1/sag101-3* (susceptible) were used as controls. Numbers of resistant leaves in 12 independent individual (T1) plants, as indicated. Black bars represent 200 μm.
(b) Basal immunity pathogen growth assay in Arabidopsis independent transgenic and wild-type and mutant control lines, as indicated. Four-week-old Arabidopsis plants were syringe-infiltrated with *Pst* DC3000 (OD_{600} = 0.0005) and bacterial titers determined at 0 dpi (empty squares; $n = 6$) and 3 dpi (filled squares; $n = 12$). Symbols of the same color represent 2 (day 0) or 4 (day 3) biological replicates in an independent experiment. Bars represent the mean of three experimental replicates ± SE. Letters indicate differences between genotypes as determined by ANOVA (Tukey HSD, $P < 0.01$).
(c) TNL (RRS1-RPS4) ETI pathogen growth assay in Arabidopsis independent transgenic and wild-type and mutant control lines, as performed in (b) but with *Pst avrRps4*.
(d) TNL (RPP4) ETI assay of Arabidopsis-independent T3 transgenic lines with wild-type and mutant controls, as indicated. Three-week-old Arabidopsis plants were spray-inoculated with *Hpa* EMWA1 (4×10^4 spores per ml) and conidiospores on leaves were quantified at 6 dpi in four independent experiments (squares; $n = 8$). Squares of the same color represent two biological replicates in an independent experiment. Letters indicate differences between genotypes as determined by ANOVA (Tukey HSD, $P < 0.05$).
(e) Number of green peach aphids per plant at 11 dpi in a no-choice assay in Arabidopsis independent transgenic and control (wild-type and mutant) lines, as indicated. Data are pooled from three independent experiments each with 10 biological replicates per experiment ($n = 30$). Squares of the same color represent 10 biological replicates in an independent experiment. Letters indicate differences between genotypes as determined by ANOVA (Tukey HSD, $P < 0.01$). Data points for Col-0, *pad4-1/sag101-3*, and *PAD4^{WT} #2* were published previously in Dongus et al. (2020).

*At*PAD4^{K380A} are not complete loss-of-function mutants and that PAD4 contains two signaling surfaces. One is located at the S118/D178 LLD pocket of PAD4 and limits GPA proliferation independently of EDS1. The other domain is located in the PAD4 EPD cavity, which confers EDS1 dimer-dependent TNL ETI and basal immunity.

SAG101 EPD cavity residues contribute to TNL ETI in Arabidopsis and wild tobacco

Recent studies show that the EDS1-SAG101 dimer is recruited by various TNL receptors to promote pathogen resistance and host cell death in ETI (Castel, Ngou, et al., 2019; Gantner et al., 2019; Lapin et al., 2019; Wu et al., 2019). We tested whether SAG101 EPD residues lining the dimer cavity are essential for its immune functions. Met304 (M304) and Arg373 (R373) of *At*SAG101 are positionally equivalent to R314 and K380 of *At*PAD4, respectively (Figures 1a and 2a; Videos S1 and S2), and are highly conserved within SAG101-containing dicot lineages (Figure 2b,c). In the *At*EDS1-*At*SAG101 crystal structure, M304 and R373 of *At*SAG101 are also exposed to the solvent (Figure 2a; Figure S7a; Video S2) (Wagner et al., 2013). As Arabidopsis PAD4 and SAG101 have non-interchangeable roles in immunity (Lapin et al., 2019; Rietz et al., 2011; Sun et al., 2021) and their C-terminal EPDs are essential for signaling (Dongus et al., 2020; Wagner et al., 2013), we tested if replacing EPD residues M304 and R373 of *At*SAG101, respectively with R314 and K380 of *At*PAD4, altered SAG101 function. *At*SAG101^{M304R} and *At*SAG101^{R373K} (*pSAG101:gSAG101-YFP*) homozygous stable transgenic lines were generated in the *pad4-1/sag101-3* mutant (Sun et al., 2021). The *At*SAG101 genomic mutant variants accumulated *in planta* (Figure S7b), had the same subcellular localization as WT SAG101-YFP in uninfected Arabidopsis (Figure S7c), and retained interaction with *At*EDS1 in *Nb* tobacco transient expression assays (Figure S7d). To measure host cell death in TNL ETI, *At*SAG101^{M304R} and *At*SAG101^{R373K} plant leaves were infiltrated with type-III secretion system equipped *Pseudomonas fluorescens* 0–1 strain (*Pf*0-1) (Thomas et al., 2009) delivering *avrRps4* (Heidrich et al., 2011; Le Roux et al., 2015). Electrolyte leakage was measured in leaves at 24 hpi as a proxy for TNL-triggered host cell death in ETI (Lapin et al., 2019). Whereas *Pf*0-1 *avrRps4* induced cell death in Col-0 and complementing *At*SAG101^{WT} *pad4-1/sag101-3* lines, *At*SAG101^{M304R}, and *At*SAG101^{R373K} lines resembled the *pad4-1/sag101-3* mutant (Figure 2d,e). In addition, in resistance assays to *Pst avrRps4*, *At*SAG101^{M304R} and *At*SAG101^{R373K} did not complement the *pad4-1/sag101-3* mutant to the level of a *pad4-1* single mutant, unlike *At*SAG101^{WT} (Figure 2f). Therefore, EPD residues M304 and R373 of *At*SAG101, which are positionally equivalent to R314 and K380 of *At*PAD4, are required both for TNL effector-triggered host cell death and pathogen resistance.

Effector-triggered immunity in *Nb* tobacco mediated by various *Solanaceae* or Arabidopsis TNL receptors utilizes *Nb*EDS1a with one of two *Nb*SAG101 isoforms (*Nb*SAG101b), and does not require *NbSAG101a* or *NbPAD4* (Gantner et al., 2019; Lapin et al., 2019). To study whether there is functional conservation of M304 and R373 of *At*SAG101 in TNL ETI, we generated mutants in the equivalent residues (M354 and R423) in *Nb*SAG101b. We tested the functionality of *Nb*SAG101b^{M354R}, *Nb*SAG101b^{R423K}, and *Nb*SAG101b^{R423A} variants using an *Nb* tobacco *pad4 sag101a sag101b* (*Nb-pss*) triple mutant (Lapin et al., 2019). These *Nb*SAG101b variants interacted with co-expressed *Nb*EDS1a in IP assays (Figure S8a) and displayed the same subcellular localization as *Nb*SAG101b^{WT} protein in *Nb* tobacco leaf cells (Figure S8b). To measure TNL ETI host cell death responses, the

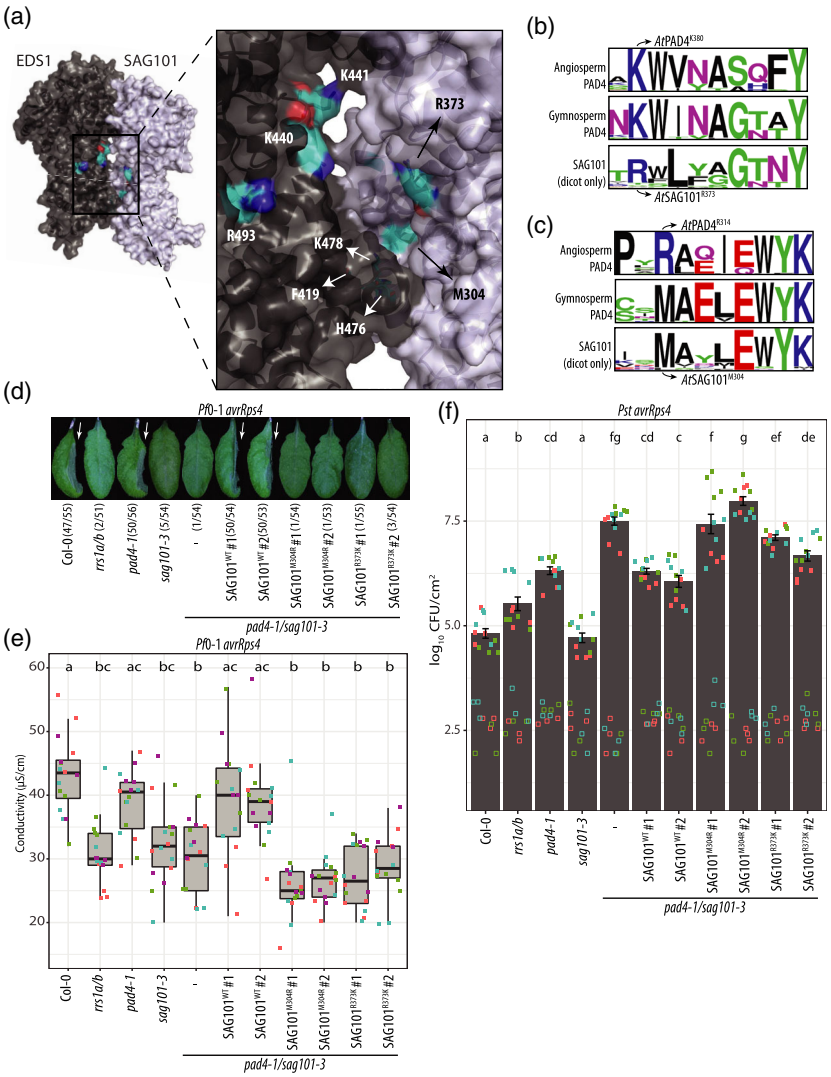

Figure 2. Contribution of *At*SAG101 conserved EP-domain residues to TNL immunity in Arabidopsis. (a) Arabidopsis EDS1-SAG101 crystal structure (Wagner et al., 2013). EDS1 (black) and SAG101 (gray) with highlighted residues previously mutated in EDS1, and M304, R373 of *At*SAG101. Highlighted residues display carbon atoms in turqoise, oxygen atoms in red, nitrogen atoms in blue and sulfur atoms in yellow (Bhandari et al., 2019; Lapin et al., 2019). See Video S2 for a 3-dimensional representation of the Arabidopsis EDS1-SAG101 cavity residues shown in (a).

(b) Sequence logos indicating the conservation of K380 of *At*PAD4 and R373 of *At*SAG101 in angiosperm and gymnosperm PAD4 and SAG101 protein sequences corresponding to $AtPAD4^{312–321}$. Protein sequences were obtained from Lapin et al. (2019).

(c) As in (b), but for R314 of *At*PAD4 and M304 of *At*SAG101. Logo corresponds to the $AtPAD4^{379–388}$ region.

(d) Macroscopic cell death in Arabidopsis independent transgenic and wild-type and mutant control lines, as indicated. Cell death was visible as tissue collapse (marked by arrowheads) at 24 hpi with *Pf*0-1 *avrRps4* (OD_{600} = 0.2) triggering TNL (RRS1-RPS4) induced host cell death. Numbers in parentheses indicate leaves showing visual tissue collapse/total infiltrated leaves per genotype. Data collected in >4 independent experiments. Pictures of one representative experiment (biological replicate) are shown.

(e) Electrolyte leakage assays quantifying host cell death in the same Arabidopsis lines as in (d) at 24 hpi with *Pf*0-1 *avrRps4* (OD_{600} = 0.2). Data are pooled from four independent experiments each with four biological replicates per experiment (n = 16). Squares in the same color represent four biological replicates in an independent experiment. Letters indicate differences between genotypes as determined by ANOVA (Tukey HSD, $P < 0.01$).

(f) TNL (RRS1-RPS4) ETI pathogen growth assay in Arabidopsis independent transgenic and wild-type and mutant control lines, as indicated. Four-week-old Arabidopsis plants were syringe-infiltrated with *Pst avrRps4* (OD_{600} = 0.0005) and bacterial titers determined at 0 dpi (empty squares; n = 6) and 3 dpi (filled squares; n = 12). Symbols of the same color represent two (day 0) or four (day 3) biological replicates in an independent experiment. Bars represent the mean of three experimental replicates ± SE. Letters indicate differences between genotypes as determined by ANOVA (Tukey HSD, $P < 0.01$).

*Nb*SAG101b variants were expressed in *Nb-pss* leaves with the *Xanthomonas campestris* pv. *vesicatoria* (*Xcv*) effector XopQ that is recognized by TNL Recognition of XopQ 1 (*Nb*ROQ1) (Adlung et al., 2016; Schultink et al., 2017). NbSAG101b^{WT} and NbSAG101b^{R423K} complemented the *Nb-pss* mutant for cell death induction at 24 hpi, whereas NbSAG101b^{M354R} behaved similarly to non-complementing YFP controls (Figure 3a). By contrast, the NbSAG101b^{R423A}

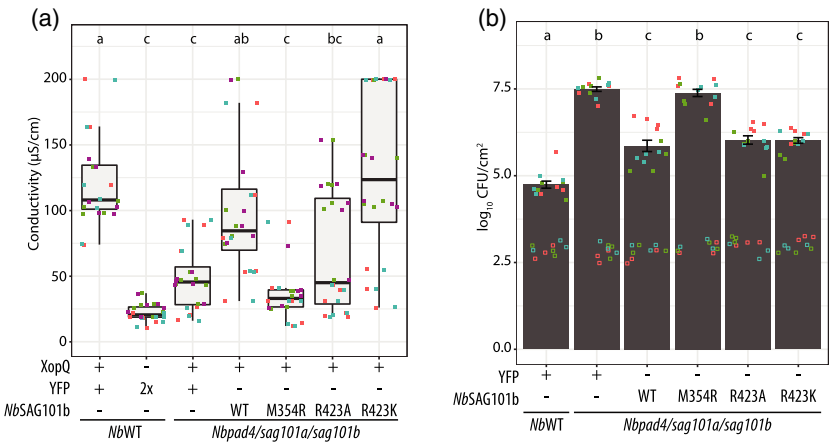

Figure 3. Impact of mutated *Nb*SAG101b conserved EP-domain residues on tobacco immune responses. (a) Electrolyte leakage assays as a measure of XopQ-triggered cell death in *Nb* tobacco WT and *epss* plants transiently expressing combinations, as indicated. YFP was used as a negative control and to normalize infiltrated OD_{600} between samples. Conductivity was measured 3 days after infiltration of *Agrobacterium tumefaciens* (*A. tumefaciens*) (OD_{600} = 0.2). Data are pooled from four independent experiments each with six biological replicates per experiment (n = 24). Squares in the same color represent six biological replicates in an independent experiment. Letters indicate differences between genotypes as determined by ANOVA (Tukey HSD, $P < 0.01$). Representative immunoblot showing protein levels of *Nb*SAG101b-YFP variants, YFP and XopQ-MYC for one experimental replicate can be found in Figure S6c.
(b) TNL (ROQ1) ETI pathogen growth assay in 5-week-old *Nb* tobacco *epss* and *Nb* tobacco WT plants at 6 dpi with *Xcv* (OD_{600} = 0.0005) after transiently expressing combinations using *A. tumefaciens* as indicated in (a). Bacterial titers were determined in four independent experiments at 0 dpi (empty squares; n = 9) and 6 dpi (filled squares; n = 12). Symbols of the same color represent two (day 0) or four (day 3) biological replicates in an independent experiment. Bars represent the mean of three experimental replicates ± SE. Letters indicate differences between genotypes as determined by ANOVA (Tukey HSD, $P < 0.01$). Representative immunoblot showing protein levels of *Nb*SAG101b-YFP variants and YFP for one experimental replicate can be found in Figure S6d.

variant partially complemented the *Nb-pss* mutant defect (Figure 3a), indicating that *Nb*SAG101b^{R423A} retains some activity in XopQ-triggered cell death. In resistance to the TNL ETI activating bacterial pathogen *Xcv* (delivering XopQ), *Nb*SAG101b^{M354R} did not complement the *Nb-pss* triple mutant whereas *Nb*SAG101^{R423K} and *Nb*SAG101^{R423A} conferred similar resistance to *Nb*SAG101b^{WT} (Figure 3b). Therefore, residue M354 in *Nb*SAG101b plays an essential role in *Nb* tobacco TNL ETI. Taken together, the data suggest functional conservation between M304 of *At*SAG101 and M354 of *Nb*SAG101b EPD cavity surface residues in Arabidopsis and *Nb* tobacco TNL ETI.

Arabidopsis PAD4 and SAG101 EPD cavity residues promote associations with RNLs and NLRs

The above data point to an essential role of M304 of *At*SAG101/M354 of *Nb*SAG101b and positionally equivalent R314 of *At*PAD4 in TNL ETI signaling. We investigated whether *At*SAG101 M304 and *At*PAD4 R314 affect EDS1 dimer molecular associations with other proteins in Arabidopsis TNL ETI. A recent study used GFP-trap purification of WT complementing YFP-PAD4 and SAG101-YFP *pad4-1/sag101-3* transgenic lines followed by liquid chromatography–mass spectrometry (LC-MS) at 6 h after *Pf*0-1 *avrRps4* infiltration of leaves (Sun et al., 2021). This allowed capture PAD4 and SAG101 interactomes before the main RRS1-RPS4 ETI transcriptional elevation of defense genes between 8 and 16 hpi (Bhandari et al., 2019; Garcia et al., 2010; Lapin et al., 2020; Mine et al., 2017; Saile et al., 2020; Sun et al., 2021). In TNL ETI-activated tissues, PAD4 associated with EDS1 (as its direct partner) and with ADR1 family RNLs, while SAG101 associated preferentially with EDS1 and NRG1 family RNLs (Sun et al., 2021). These interactions tally with genetic co-functions of EDS1-PAD4 with ADR1s in ETI and basal immunity and EDS1-SAG101 with NRG1s in TNL ETI (Lapin et al., 2019; Pruitt et al., 2021; Sun et al., 2021; Wu et al., 2019).

We compared the *At*SAG101^{M304R} and *At*PAD4^{R314A} interactomes with WT *At*SAG101 and *At*PAD4 in *pad4-1/sag101-3* at 6 h after infiltration with *Pf*0-1 *avrRps4* bacteria. To obtain higher levels of PAD4 bait protein for the LC-MS work, we made use of the genomic *At*PAD4 lines (gPAD4^{WT} and gPAD4^{R314A}) in *pad4-1/sag101-3* described above (Figure S3) (Bhandari et al., 2019). *Pf*0-1 *avrRps4* bacteria were infiltrated into leaves of Arabidopsis transgenic lines *gPAD4^{WT} #1*, *gPAD4^{R314A} #1*, *SAG101^{WT} #2*, and *SAG101^{M304R} #1*, and a *p35S:YFP-StrepII-3xHA* line (YFP-SH in Col-0) as control for YFP non-specific protein binding (Sun et al., 2021). Leaf samples were harvested at 6 hpi. The bait proteins were purified from soluble leaf extracts using GFP-trap agarose beads and co-purified proteins analyzed by LC-MS. Similar amounts of *At*PAD4^{WT} compared with *At*PAD4^{R314A} and *At*SAG101^{WT} compared with *At*SAG101^{M304R} protein were used for the interactome analysis, as measured by immuno-detection of input samples and normalized bait protein abundances in LC-MS

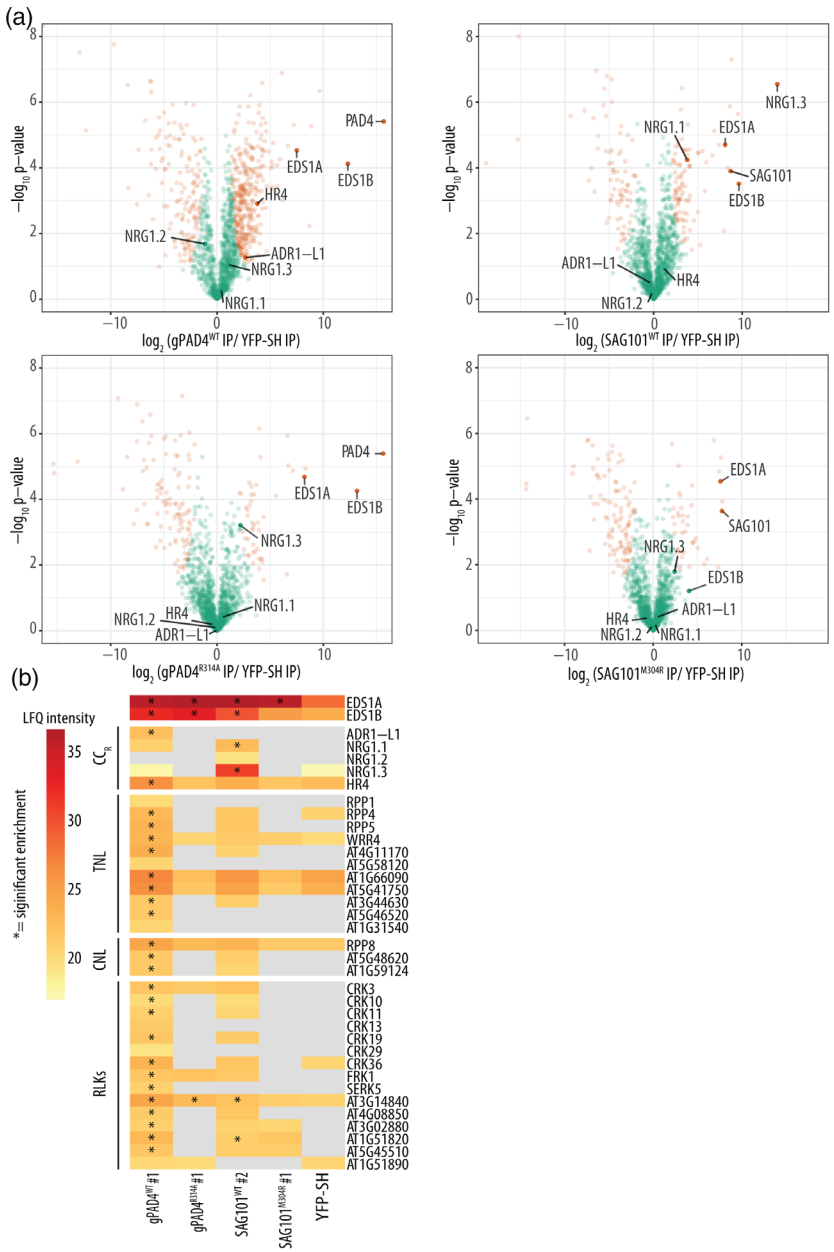

Figure 4. Protein interactome analysis of Arabidopsis lines expressing wild type and EP-domain signaling mutants of PAD4 or SAG101. (a) Volcano plots of normalized protein abundance (label-free quantitation [LFQ], log_2-scaled) for proteins co-purified with YFP-gPAD4^{WT} (top left), YFP-gPAD4^{R314A} (bottom left), SAG101^{WT}-YFP (top right), and SAG101^{M304R}-YFP (bottom right) from total leaf extracts of T3 stable Arabidopsis transgenic lines infiltrated with *Pf*0-1 *avrRps4* (6 hpi, OD_{600} = 0.2). Proteins significantly enriched relative to YFP-SH are shown in orange in the top right corner of each plot. As a cut-off for significant interactions we used the following threshold: protein was detected in three of four experiments; $|log_2$ (bait protein IP/YFP-SH IP)$| \geq 1$, $P \leq 0.05$. Missing values were imputed. See Table S1 and Materials and methods for IP-MS peptide data analysis from four biological replicates per sample.
(b) Heat map representation of the LFQ for CC_R domain-containing proteins, NLRs belonging to the TNL and CNL subgroups, and RLKs identified in the MS experiment. Asterisks indicates significant interactions relative to YFP-SH (for significance see a). Gray blocks indicate the protein was not detected in the sample. See Table S1 and Materials and methods for IP-MS peptide data analysis from four biological replicates per sample.

(Figure S9; Table S1). In addition, WT and mutant *At*PAD4 and *At*SAG101 samples co-purified similar amounts of the functional native EDS1A isoform in Col-0 (Figure S9b; Table S1) (Wagner et al., 2013). These measurements ensured that interactome differences would not be caused by large differences in dimer abundance of EPD mutant versus WT EDS1A-PAD4 and EDS1A-SAG101.

In line with a previous analysis (Sun et al., 2021), *At*PAD4^{WT} and *At*SAG101^{WT} co-purified multiple NLRs, including respective ADR1 and NRG1 RNL family

members, and several RLKs not detected in YFP-SH samples (Figure 4; Table S1). More NLRs and RLKs were enriched statistically significantly in *At*PAD4^{WT} compared with *At*SAG101^{WT} samples (identified in three of four replicates with $P < 0.05$, relative to YFP-SH), as indicated by orange circles in Figure 4a and asterisks in Figure 4b (Sun et al., 2021). Notably, NLRs and RLKs that were identified in *At*PAD4^{WT} and *At*SAG101^{WT} were either not detected or not enriched in *At*PAD4^{R314A} and *At*SAG101^{M304R} relative to YFP-SH samples (Figure 4a,b). Compared with *At*PAD4^{WT} and *At*SAG101^{WT}, the EPD cavity mutants *At*PAD4^{R314A} and *At*SAG101^{M304R} did not associate stably with RNLs ADR1-L1 and NRG1.1, respectively (Figure 4a,b). In addition, *At*SAG101^{M304R} failed to enrich an N-terminally truncated NRG1.3 isoform, which associates with *At*SAG101^{WT} protein (Figure 4a,b) (Sun et al., 2021). Moreover, *At*PAD4^{WT} but not signaling-deficient *At*PAD4^{R314A} or *At*SAG101^{WT} enriched significant amounts of the CC_R-(HeLo) domain RPW8 homolog, HR4 (Figure 4) (Berkey et al., 2017; Xiao et al., 2003, 2005). These data suggest that *At*PAD4 and *At*SAG101 EPD cavity surface residues that are not in direct contact with EDS1 in each dimer (Figures 1a and 2a; Figures S1a, S2a, and S7a; Videos S1 and S2) contribute to associations with specific RNL subtypes, certain NLRs and, in the case of *At*PAD4, RLKs and RPW8-like HR4.

The differential associations of *At*PAD4^{WT} or *At*SAG101^{WT} compared with their EPD mutant variants could be explained by differences in immune-related gene expression of associated proteins between the genotypes. For RNLs *ADR1-L1* and *NRG1.1*, TNL *RPP1* and CNL *RPP8*, we did not observe significant differences in gene expression between *At*PAD4^{WT} and *At*PAD4^{R314A} or between *At*SAG101^{WT} and *At*SAG101^{M304R} at 0 or 6 hpi with *Pf*0-1 *avrRps4* (Figure S10). This suggests that M304 of *At*SAG101 and R314 of *At*PAD4 are important for mediating direct or indirect interactions with various NLR proteins post-transcriptionally. In contrast, there were significant changes in gene expression between WT and mutant genotypes at 0 and 6 hpi with *Pf*0-1 *avrRps4* for RLK *Cysteine-rich RLK 36* (*CRK36*), suggesting that reduced CRK36 association with PAD4^{R314A} and SAG101^{M304R} might be due to diminished *CRK36* expression. Taken together, the LC-MS results show that *At*PAD4 and *At*SAG101 EPD cavity surfaces within EDS1 dimers have an essential role in immunity signaling and forming specific associations with immunity components.

DISCUSSION

Exclusive dimers between EDS1 and its two sequence-related partners SAG101 and PAD4 connect immune receptor activation by pathogens to the induction of host defenses (Dongus & Parker, 2021; Lapin et al., 2020). Protein structure-guided analyses identified EPDs of EDS1-family proteins (PFAM: PF18117) as essential for signaling (Bhandari et al., 2019; Dongus et al., 2020; Gantner et al., 2019; Lapin et al., 2019; Sun et al., 2021; Wagner et al., 2013). In Arabidopsis, EDS1-SAG101 dimers control TNL-mediated ETI responses by forming induced complexes with NRG1 family RNLs (Lapin et al., 2019; Sun et al., 2021). By contrast, EDS1-PAD4 dimers associate preferentially with ADR1 family RNLs to promote a basal immunity branch through which TNL and CNL receptors, and some cell-surface PRRs, signal to induce an anti-pathogen defense (Castel, Ngou, et al., 2019; Dongus & Parker, 2021; Pruitt et al., 2021; Saile et al., 2020; Sun et al., 2021; Wu et al., 2019; Wu, Tian, Liu, Zhang, & Li, 2021). A number of conserved EDS1 EPD residues lining a cavity formed by each dimer were found to be important both for dimer association with RNLs and immunity functions (Bhandari et al., 2019; Gantner et al., 2019; Lapin et al., 2019; Sun et al., 2021). It was not known whether the EPD cavities of SAG101 or PAD4 have a direct role in EDS1 EPD-specified resistance and protein associations. We identify here EPD cavity residues of *At*PAD4 and *At*SAG101/*Nb*SAG101b that determine respective EDS1 dimer-specific associations with RNLs and pathogen immunity in ETI-activated tissues. This finding is significant because it suggests that similar but non-identical C-terminal EPD cavity surfaces in SAG101 and PAD4 underlie EDS1 dimer functional specificity in immunity signaling. We propose that SAG101 and PAD4 EPD domain cavity residues might help to create the distinctive character of each EDS1 dimer defense branch observed in TNL ETI (Figure 5).

We located two residues at the same structurally aligned EPD positions in *At*PAD4 (R314 and K380) and *At*SAG101 (M304 and R373) that are necessary for immunity signaling by each branch (Figures 1, 2, and 4) but not for stable dimer formation or subcellular localization (Figure 4; Figures S2, S4c, and S7c,d). Generally lower accumulation of PAD4 EPD mutant forms, particularly PAD4^{K380A}, compared with WT PAD4 protein in *Nb* transient assays and Arabidopsis stable transgenic lines (Figures S2a, S3d, and S5b) suggests that an intact EPD cavity surface stabilizes PAD4, perhaps through basal association with immunity components in non-infected tissues. We cannot rule out that PAD4^{K380A} low accumulation in part accounts for its failure to signal in the immune response. R314 and K380 of *At*PAD4 as well as M304 of *At*SAG101 are conserved across PAD4- and SAG101-containing angiosperm lineages, whereas R373 of *At*SAG101 is less conserved (Figure 2b,c). A requirement for M354 of *Nb*SAG101b, which is equivalent to M304 of *At*SAG101, in *Nb* tobacco TNL Roq1-induced cell death and bacterial resistance (Figures 2c and 3a,b), suggests that this methionine has a conserved essential role in SAG101 EPD cavity-specified TNL ETI. It is significant that R314 and K380 of *At*PAD4 were not functionally interchangeable with a different positively charged

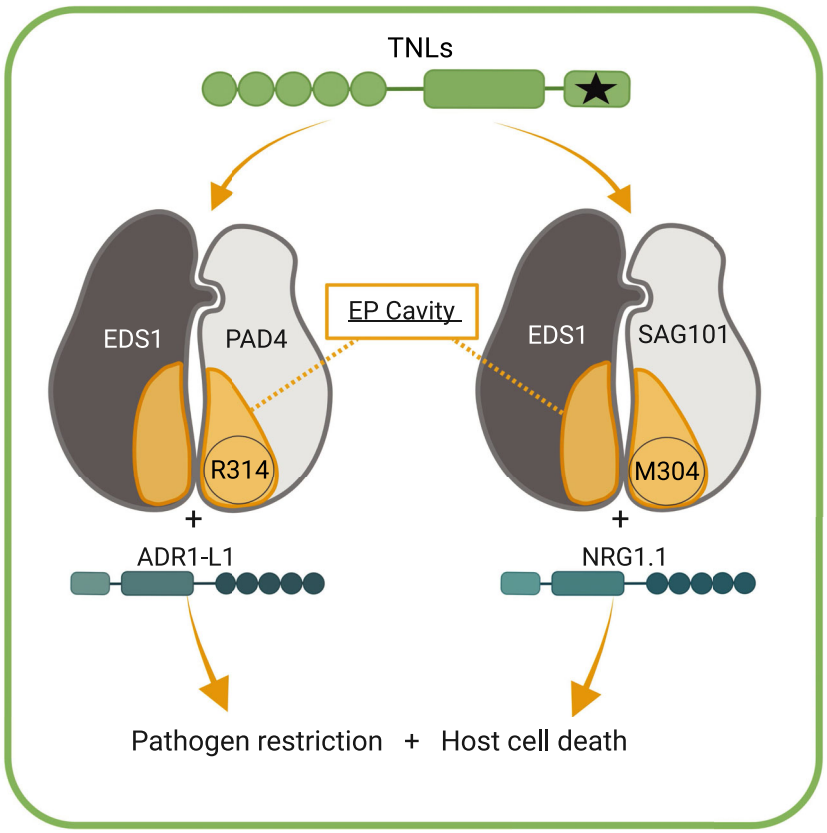

Figure 5. Graphical summary showing the roles of the EDS1-PAD4 and EDS1-SAG101 heterodimer cavities (highlighted in orange) in Arabidopsis TNL immunity.
The EDS1-PAD4 dimer promotes mainly pathogen restriction, and contributes weakly to host cell death. The EDS1-SAG101 dimer promotes host cell death, and contributes weakly to pathogen restriction. PAD4 and SAG101 require EPD cavity residues R314 and M304, respectively, to induce resistance and host cell death. Black star depicts a TNL receptor TIR domain NADase activity necessary for downstream engagement of EDS1 dimers. Our results suggest that precise PAD4 and SAG101 EPD amino acid coordinates define the two EDS1 dimer functions as well as their specific associations with HeLo-domain helper NLRs (e.g., ADR1-L1 and NRG1.1 shown) and a number of other immunity components. Hence, EDS1 partners contribute an essential signaling surface to mobilize EDS1-dependent pathogen immunity.

residue (respectively, lysine and arginine) or with the positionally equivalent residues M304 and R373 of *At*SAG101 (Figure 2d–f; Figure S5) (Gantner et al., 2019; Lapin et al., 2019). This suggests that precise PAD4 and SAG101 amino acid coordinates underlie immunity functions of the two EDS1 heterodimers, perhaps for specific modifications and/or interactor binding. The PAD4 and SAG101 EPD mutant phenotypes presented here also support earlier findings that EDS1 is inactive without one or other of its direct partners (Cui et al., 2017; Rietz et al., 2011; Wagner et al., 2013) and hence EDS1 immunity functions are defined by the heterodimer surfaces.

The above data raise an important question of which protein or molecule directly binds to the structurally similar but non-identical EDS1-SAG101 and EDS1-PAD4 EPD cavities. Recent biochemical studies and the resolved cryo-electron microscopy structures of two pathogen effector-activated TNL receptor oligomers (Arabidopsis RPP1 and *Nb* tobacco ROQ1) reveal that some TIR domain proteins and TNL receptors hydrolyze oxidized nicotinamide adenine dinucleotide (NAD^+) after self-association, producing dinucleotide-ribose derivatives (Bayless & Nishimura, 2020; Horsefield et al., 2019; Lapin et al., 2022; Ma et al., 2020; Martin et al., 2020; Wan, Essuman, et al., 2019). Effector-induced RPP1 tetramerization assembles an active NADase enzyme, and it was proposed that one or more TIR-generated NAD^+ hydrolysis products are signaling intermediates for downstream defense (Bayless & Nishimura, 2020, Horsefield et al., 2019, Lapin et al., 2022, Ma et al., 2020, Martin et al., 2020, Wan, Essuman, et al., 2019). Plant TIR domains can also synthesize 2′,3′-cyclic nucleotide monophosphates signaling via EDS1 (Yu et al., 2021). Because tested TIR proteins and TNLs trigger immune and/or cell death responses via *EDS1* (Lapin et al., 2020), and EDS1-SAG101 or EDS1-PAD4 dimers are the minimal functional units for TNL- and TIR-triggered defense (Bhandari et al., 2019; Cui et al., 2017; Lapin et al., 2020; Sun et al., 2021) (this study), a TIR- or TNL-produced small molecule would be a candidate for dimer EPD cavity binding. Cooperative binding of a small molecule by EDS1-PAD4 and EDS1-SAG101 dimers might enable recruitment of specific RNL subfamilies, thereby conferring distinctive immunity outputs (Figure 5).

The TNL- or TIR-activated RNLs are further candidates for EPD cavity direct binding (Sun et al., 2021, Wu, Tian, Liu, Zhang, & Li, 2021). Current evidence suggests that Arabidopsis ADR1 and NRG1 family RNLs operate as induced oligomers, which associate with and form pores at the plasma membrane via exposed N-terminal CC_R/HeLo-domain α-helices (Jacob et al., 2021). It is possible that

activated RNLs behave like the pathogen-activated Arabidopsis CNL pentamer, ZAR1, which forms Ca^{2+}-permeable inward channels at the plasma membrane using its exposed N-terminal α1 helices (Bi et al., 2021; Parker et al., 2021; Wang, Hu, et al., 2019; Wang, Wang, et al., 2019). Pore-forming activities have also been reported for HeLo-domain containing animal and fungal MLKL, HET-S, and HELLP proteins (Daskalov et al., 2016; Feehan et al., 2020; Petrie et al., 2019). Members of a family of Arabidopsis MLKLs form tetramers, which can move along microtubules close to the plasma membrane, and they contribute to basal immunity independently of host cell death (Mahdi et al., 2020). For plant RNLs and MLKLs, cell death is probably an extreme output that might not reflect their primary immunity functions. In *Nb* tobacco TNL ETI assays, induced Arabidopsis EDS1-SAG101 association with NRG1.1 leading to host cell death required an oligomerization-competent NRG1 protein but not predicted N-terminal α-helix "pore" residues (Sun et al., 2021). It is interesting that EDS1-SAG101 association with a truncated NRG1 isoform, NRG1.3, observed by Sun et al. (2021) and in the present study, is lost with the EDS1-SAG101^{M304R} dimer (Figure 4; Figure S9b; Table S1). NRG1.3 is a negative regulator of the EDS1-SAG101–dependent TNL immunity (Wu, Tian, Liu, Huang, et al., 2021), and therefore might compete with active NRG1.1 and NRG1.2 proteins for EDS1-SAG101 association to dampen this defense branch. Considering these data, we think it likely that EDS1-SAG101 and EDS1-PAD4 dimers, via their EPD cavities, provide crucial regulation of NRG1 and ADR1 to execute defenses.

Arabidopsis EDS1-SAG101 dimer signaling with the NRG1 family RNLs is closely aligned to TNL-mediated ETI. By contrast, Arabidopsis EDS1-PAD4 dimers with ADR1 family RNLs are recruited more broadly to promote the basal immunity branch of ETI initiated by TNL and some CNL receptors, and PTI defenses initiated by the plasma membrane-anchored PRR, RLP23 (Dongus & Parker, 2021; Lapin et al., 2020; Pruitt et al., 2021; Tian et al., 2021). All of these triggers require the EDS1 EPD cavity surface for signaling. Hence, the EDS1-PAD4-ADR1 node appears to integrate signals from intracellular NLRs and cell surface PRRs, using the EDS1-PAD4 EPDs. Future studies will assess whether this convergent action of EDS1-PAD4 dimers with ADR1s involves the TIR domain or TNL proteins (Tian et al., 2021), and thus potentially a TIR-generated small molecule. Arabidopsis PAD4 has additional signaling roles that are independent of EDS1 in silicon-induced resistance against powdery mildew and in resistance to the leaf-sucking insect GPA (Louis & Shah, 2015; Pegadaraju et al., 2007; Wang et al., 2020). While the PAD4 EPD cavity is essential for pathogen immunity (Figure 1b–d, Figure S3), it is dispensable for PAD4-mediated GPA resistance (Figure 1e). This finding is in line with GPA resistance being conferred by the N-terminal PAD4 LLD alone (Dongus et al., 2020; Louis et al., 2012; Louis & Shah, 2015). It further highlights that PAD4^{R314A} and PAD4^{K380A} EPD cavity mutants are not complete loss-of-function mutants. Taken together, the results show that Arabidopsis PAD4 contains two separable signaling surfaces, one at the C-terminal PAD4 EPD cavity and the other located at the N-terminal LLD catalytic pocket.

Our IP-MS analysis of Arabidopsis WT PAD4 and SAG101 and corresponding EPD mutants *At*PAD4^{R314A} and *At*SAG101^{M304R} (Figure 4, Figure S9) was designed to detect interacting proteins for each dimer after Arabidopsis TNL (RRS1-RPS4) activation and before major transcriptional changes (Bhandari et al., 2019; Garcia et al., 2010; Saile et al., 2020; Sun et al., 2021). Quantitation of IP-MS peptide profiles showed that amounts of IPed *At*PAD4^{R314A} and *At*SAG101^{M304R} and co-purified EDS1A were similar to their WT counterparts (Figure 4, Figure S9b; Table S1). This suggests that a substantial portion of reduced or lost associations was caused by EPD defects in the respective heterodimers. The data show that both EDS1 partner EPD cavity surfaces are important for promoting dimer interactions with specific RNL subfamilies (Figure 4) (Sun et al., 2021). Significantly, we detected another HeLo-domain protein, HR4, associating with PAD4 but not SAG101 in an EPD-dependent manner (Figure 4). HR4 is one of four RPW8-family paralogs (HR1–HR4) in Arabidopsis accession Col-0, where it replaces RPW8.1 and RPW8.2 that are present in other accessions and represent a major polymorphic source of resistance to powdery mildew disease (Berkey et al., 2017; Xiao et al., 2001). RPW8/HRs are small membrane-binding proteins with a CC_R-domain. Arabidopsis RPW8.1 and RPW8.2 promote *EDS1*- and *PAD4*-dependent basal immunity to powdery mildew fungi and other pathogens (Berkey et al., 2017; Castel, Wu, et al., 2019; Xiao et al., 2001, 2004). Tested RPW8 and HR proteins accumulate at host membrane sites around fungal infection structures (haustoria) (Berkey et al., 2017; Wang et al., 2009). As an EDS1-PAD4 pool associates with plasma membrane-anchored immunity components, such as RLKs (Pruitt et al., 2021; Sun et al., 2021; this study), we speculate that RPW8-like protein association and co-function with EDS1-PAD4 might contribute to the basal immune response. HR4 was detected as a high-confidence EDS1-PAD4 interactor in this analysis and by Sun et al. (2021), but not in PAD4 IP-MS assays of mock or RLP23-triggered tissues (Pruitt et al., 2021). The role of HR4 relative to other RPW8 paralogs in resistance remains obscure, although HR4 is maintained in Arabidopsis accessions and therefore probably has some defense and/or fitness value (Xiao et al., 2004; Barragan et al., 2019). Some HR4 alleles elicit autoimmunity (hybrid incompatibility) when combined with specific alleles of the CNL receptor, RPP7 (Chae et al., 2014). Moreover, HR4 from Arabidopsis

accession Fei-0 promotes oligomerization of an RPP7 protein from accession Lerik-1, which leads to cell death in *Nb* tobacco transient assays (Li et al., 2020). Hence, HR4 might be guarded by RPP7 as an RPW8 decoy or basal immunity component. Establishing here that EDS1-PAD4 interacts with HR4 suggests that HR4 in some way regulates EDS1-PAD4-ADR1 defense node activity.

We also detected EPD-dependent dimer associations with NLR proteins (TNLs and CNLs) as well as numerous non-NLR immunity components (Figure 4b; Table S1). Specific interactions between TNLs and EDS1 and PAD4 have been reported (Bhattacharjee et al., 2011; Heidrich et al., 2011; Kim et al., 2012; Huh et al., 2017; Zhang et al., 2019). How these relate to TNL oligomerization and NADase activity, which in the case of RPP1 occurs without EDS1-family proteins (Ma et al., 2020), is not known. The EPD-dependent PAD4 and SAG101 high-confidence interactors detected here (Figure 4; Table S1) and in a previous study (Sun et al., 2021) likely reflect dynamic sites and modes of action of the EDS1 dimers. It is increasingly evident that immune-responding cells and organelles become reorganized during ETI well before cell permeabilization and eventual death (Bi et al., 2021; Jacob et al., 2021; Zavaliev et al., 2020). This might enable orchestrated protein complexes to assemble transiently for particular immunity outputs. In Arabidopsis, cells bordering ETI foci is a likely place where EDS1-PAD4 and ADR1-dependent "basal" defense reprogramming is most relevant for local defense reinforcement and systemic resistance (Bonardi et al., 2011; Lapin et al., 2020).

EXPERIMENTAL PROCEDURES

Plant materials, growth conditions, and pathogen strains

Arabidopsis *pad4-1*, *sag101-3*, and *eds1-2* mutants are in the Col-0 background and were previously described (Wagner et al., 2013), as were the transgenic lines *pPAD4:StrepII-YFP-PAD4* (in *pad4-1/sag101-3*) (Bhandari et al., 2019; Dongus et al., 2020), pSAG101:gSAG101-YFP (in *pad4-1/sag101-3*), and pPAD4:YFP-Linker-gPAD4:downstream(ds)PAD4 (in *pad4-1/sag101-3*) (Sun et al., 2021) (see Table S2 for primers). *Pseudomonas syringae* pv. *tomato* (*Pst*) strain DC3000 and *Pst avrRps4* were described previously (Cui et al., 2017) as was the type III secretion system equipped *Pseudomonas fluorescens* 0–1 (*Pf*0-1) delivering *avrRps4* (Thomas et al., 2009). Plants were grown on soil in a controlled environment and insect-free chambers under a 10-h light/14-h dark regime (photosynthetically active radiation: 100–150 μmol m^2 sec^{-1}) at 22°C and 60% relative humidity.

Pathogen infection assays in Arabidopsis

For bacterial growth assays, *Pst* DC3000 or *Pst avrRps4* (OD_{600} = 0.0005 (Hinsch & Staskawicz, 1996) in 10 mM $MgCl_2$ was hand-infiltrated into leaves of 4-week-old plants. Bacterial titers were measured at 3 h post-infiltration (day 0) and 3 days, as described previously (Lapin et al., 2019). Each biological replicate consisted of three leaf disks from different plants and data shown in each experiment are compiled from two to four biological replicates, as described in the figure 1, 2 and S3 legends. Statistical analysis was performed using one-way ANOVA with multiple testing correction using Tukey's HSD (*P*-value as described in figure 1, 2 and S3 legends). For cell death assays, *Pf0-1 avrRps4* (OD_{600} = 0.2) in 10 mM $MgCl_2$ (syringe infiltration) or 10 mM $MgCl_2$/0.01% Silwet-L77 (vacuum infiltration) was infiltrated into leaves of 4-week-old plants (Heidrich et al., 2011; Le Roux et al., 2015; Thomas et al., 2009). Macroscopic cell death phenotypes were recorded 24 h after hand infiltration of the half leaves. For ion leakage assays, leaves were vacuum-infiltrated, and the electrolyte leakage was measured at 0 and at 24 hpi as described previously (Lapin et al., 2019). Each biological replicate consisted of two leaf disks from four different plants and data shown are compiled from four biological replicates. Statistical analysis was performed as described in figure 2 legend.

The *Hpa* isolate, EMWA1, was sprayed on to 3-week-old plants at 4×10^4 spores per ml of dH_2O. For microscopic disease phenotypes, leaves were stained with lactophenol Trypan blue (Koch & Slusarenko, 1990; Muskett et al., 2002) by boiling leaves for 1 min in Trypan blue solution (1:1 diluted with 100% ethanol) and destaining with chloral hydrate (2.5 g ml^{-1} ddH_2O) for >24 h. To quantify *Hpa* sporulation on leaves, one pot with approximately 10 plants per genotype were infected and treated as a biological replicate, with two biological replicates per independent experiment. Plants were harvested at 6 dpi and plant fresh weight was determined. Conidiospores were suspended in 5 ml dH_2O and counted under a light microscope using a Neubauer counting chamber. Statistical analysis was performed using one-way ANOVA with multiple testing correction using Tukey's HSD (*P*-value as described in figure 1 and S3 legend).

For gene expression analysis in Figure S4, leaves of 4-week-old plants were hand-infiltrated with mock (10 mM $MgCl_2$) or bacteria (OD_{600} = 0.005) and samples were taken at 24 hpi. *ACT2* was used as a reference gene (see Table S2 for primers). The data shown are results from three independent experiments each with two to three biological replicates. For analysis of gene expression in samples for the IP-MS experiment (Figure S9), data shown represent one biological replicate from four independent experiments.

Pathogen infection assays in *Nicotiana benthamiana*

Xanthomonas campestris pv. *vesicatoria* (85–10; also *Xanthomonas euvesicatoria*) (Thieme et al., 2005) infection assays in the presence of *A. tumefaciens* were performed as described previously (Lapin et al., 2019). *Agrobacterium tumefaciens* strains (OD_{600} = 0.2) were prepared as for the transient expression assays, including a P19 expressing strain, where *Xcv* was added at final OD_{600} = 0.0005. To ensure equal OD_{600} in all samples, *A. tumefaciens* expressing *p35S:YFP* was used in all experiments as filler. Leaves of 5-week-old *N. benthamiana* plants were hand-infiltrated and at day 0 (3 hpi) and day 6 samples were taken to measure bacterial growth. XopQ-induced cell death was induced by *A. tumefaciens*-mediated *transient expression of p35S:XopQ-MYC* (OD_{600} = 0.2) (Adlung et al., 2016; Lapin et al., 2019). Samples for ion leakage measurements were taken at 3 dpi and conductivity was measured 6 h later. Statistical analysis was performed using one-way ANOVA with posthoc Tukey's HSD involving multiple testing correction (*P*-value as described in figure 3 legend).

Aphid no-choice bioassay in Arabidopsis

GPA fecundity assays were performed as described previously (Nalam et al., 2018). For each biological replicate, five 1-day-old nymphs were released on to the center of a 17-day-old plant. The total number of aphids (adult + nymphs) per biological replicate

were counted 11 days post-infestation. Each independent experimental replicate consisted of 10 biological replicates per genotype. Statistical analysis was performed using one-way ANOVA with multiple testing correction using Tukey's HSD (*P*-value as described in figure 1 legends).

Plasmid constructs

*At*PAD4, *At*SAG101, and *Nb*SAG101b mutant variants were obtained by site-directed mutagenesis on previously published pENTR/D-TOPO *cPAD4*, *pSAG101:gSAG101-YFP*, and *p35S:NbSAG101b-GFP* according to the QuikChangeII site-directed mutagenesis manual (Agilent, Santa Clara, CA, USA) (see Table S2 for primers) (Bhandari et al., 2019; Lapin et al., 2019; Wagner et al., 2013). Mutations generated by site-directed mutagenesis PCR were verified by sequencing. cPAD4 was recombined by an LR reaction into a pAM-PAT-based binary vector backbone to create *pPAD4:StrepII-YFP-cPAD4* (Bhandari et al., 2019; Witte et al., 2004). Genomic PAD4 (gPAD4; *pPAD4:YFP-Linker-gPAD4:dsPAD4*) was cloned by performing a PIPE-PCR on genomic Col-0 DNA and were recombined into a pDONR201 vector by competent DH10b cells (Klock & Lesley, 2009). Using PIPE-PCR YFP and a Linker (9xAla-Gly) were introduced in front of the PAD4 start codon (ATG) to create an in-frame YFP-Linker-PAD4 (YFP-gPAD4) fusion protein. YFP-gPAD4 mutant variants were created by site-directed mutagenesis on pDONR201 *YFP-gPAD4* according to the QuikChangeII site-directed mutagenesis manual (Agilent) (see Table S2 for primers). To create an expression clone, pDONR 201 YFP-gPAD4 was recombined using an LR reaction into the pAlligator2 (without *p35S*) (Jang et al., 2009) binary vector (Bensmihen et al., 2004). *p35S:AtEDS1-3xFLAG*, *p35S:AtEDS1*$^{LLIF > AAAA}$*-3xFLAG* (Bhandari et al., 2019; Wagner et al., 2013), and *p35S:XopQ-4xMYC* (Adlung et al., 2016) were published previously. *Nb*EDS1a (Niben101Scf06720g01024.1) was cloned into pENTR/D-TOPO with introns from the start ATG codon until the stop codon using genomic DNA as a template and then LR-recombined into pXCSG-3xFLAG (Witte et al., 2004) to obtain the *p35S:NbEDS1a-3xFLAG* expression vector.

Generation of transgenic Arabidopsis plants

Stable transgenic lines were generated by transforming a binary expression vector (containing Basta resistance for PAD4 and gSAG101 clones, seed fluorescence for gPAD4 clones) into Arabidopsis null mutant *pad4-1/sag101*-3 (Wagner et al., 2013), using *Agrobacterium*-mediated (*A. tumefaciens* GV3101 pMP90 RK) floral dipping (Logemann et al., 2006). After selecting single-insert, homozygous transgenic lines, all lines were genotyped for *pad4-1/sag101-3* and by sequencing for the presence of the correct transgene before performing pathogen assays.

Transient expression of proteins in *Nicotiana benthamiana*

Nicotiana benthamiana plants for *A. tumefaciens*-infiltration assays were grown under long-day conditions (24°C) for 5–6 weeks. Transient protein expression in *N. benthamiana* for co-immunoprecipitation (co-IP) and confocal microscopy was performed by co-infiltrating *A. tumefaciens* cells carrying constructs at an OD_{600} of 0.4–0.6 in a 1:1 ratio. Before syringe infiltration, *A. tumefaciens* cells were incubated for 1–3 h at 28°C in induction buffer (150 μM acetosyringone, 10 mM MES pH 5.6, 10 mM $MgCl_2$) and mixed at 650 rpm in an Eppendorf Thermomixer. Leaf samples from *N. benthamiana* were harvested at 3 dpi for confocal microscopy, and for co-IP samples were snap frozen in liquid nitrogen and stored at −80°C before processing. To determine protein expression in *Xcv* resistance and XopQ cell death assays, leaf samples were taken at 2 dpi snap frozen in liquid nitrogen and stored at −80°C before processing.

Microscopy and imaging

For *At*PAD4 and *At*SAG101 subcellular localization in Arabidopsis, leaves of 4-week-old plants were hand-infiltrated with, respectively, *Pst AvrRps4* (OD_{600} = 0.005) or *Pf0-1 avrRps4* (OD_{600} = 0.2) and protein localization was determined at 24 hpi. For *Nb*SAG101b subcellular localization in *Nb* tobacco, confocal microscopy was performed 3 days after transient expression using *A. tumefaciens*. For confocal laser scanning microscopy, leaf disks were transferred to glass slides and covered in ddH_2O. TSC SP8 confocal microscope (Leica) was used with the following setup: 20× water objective, (HC PL APO CS2 20×, 0.75 IMM), argon laser YFP excitation at 514 nm, detection between 518 and 530 nm, and autofluorescence of chlorophyll A detection between 695 and 737 nm. Confocal images were compiled using Fiji (ImageJ). Microscopic *Hpa* colonization, hypersensitive response, and trailing necrosis (disease phenotypes) were documented using a Zeiss Axio Imager microscope.

Protein extraction, co-IP, and Western blotting

Total leaf extracts were ground to a fine powder and processed in extraction buffer (50 mM Tris pH 7.5, 150 mM NaCl, 10% [v/v] glycerol, 2 mM EDTA, 5 mM DTT, 0.1% Triton X-100, and protease inhibitor [Roche, Mannheim, Germany, 1 tablet per 50 ml]). Lysates were centrifuged for 20 min, 21 000 ***g*** at 4°C. Supernatant was used as input sample (50 μl). IPs were conducted by incubating the input sample (1.2 ml) with 10 μl GFP TrapA (gta100; Proteintech, Planegg-Martinsried, Germany) for 3 h at 4°C. Beads pelleted by centrifugation and washed four times in extraction buffer. Protein (input samples or ground-leaf tissue) or IP samples were boiled at 96°C in 2× Laemmli buffer for 10 min. Proteins were separated by sodium dodecyl sulfate–polyacrylamide gel electrophoresis and analyzed by immunoblotting using primary antibodies α-GFP (11 814 460 001; Roche), α-FLAG (F7425; Sigma-Aldrich, Merck KGaA, Darmstadt, Germany) and α-MYC (2278; Cell Signaling Technologies), and horseradish peroxidase-conjugated antibodies (A9044 and A6154; Sigma-Aldrich). Antibodies were used in dilution 1:5000 in Tris-buffered saline + Tween20 with 2% non-fat milk powder and 0.01% (v/w) sodium azide.

IP of YFP-gPAD4$^{WT/R314A}$ and SAG101$^{WT/M304R}$-YFP in Arabidopsis for IP-MS

IP-MS protocol was performed as described previously (Sun et al., 2021). Five-week-old Arabidopsis plants containing *p35S:StrepII-3xHA-YFP* (Col-0), *pPAD4:YFP-gPAD4*$^{WT\#1/R314A\#1}$ (*pad4-1 sag101-3* background), or *pSAG101:gSAG101*$^{WT\#2/M304R\#1}$*-YFP* (*pad4-1 sag101-3*) were vacuum infiltrated with *Pf0-1 avrRps4* bacteria (OD_{600} = 0.2 in 10 mM $MgCl_2$ with 0.01% Silwet L-70). Two grams of rosette material was collected at 6 hpi, snap-frozen in liquid nitrogen and kept at −80°C until IP. On the day of IP, samples were ground to fine powder in Precellys 15 ml tubes (P000946-LYSK0-A; Bertin Instruments, Montigny-le-Bretonneux, France). The protein extraction was performed in 10 ml of the buffer composed of 20 mM PIPES–KOH pH 7.0, 150 mM NaCl, 10 mM $MgCl_2$, 10% glycerol (v/v), 5 mM DTT, 1% Triton X-100, Plant Protease Inhibitor cocktail (11873580001; Millipore Sigma, Merck KGaA, Darmstadt, Germany). The protein extraction was performed at 4°C for 20 min under constant end-to-end mixing (approximately 60 rpm). Subsequently, the samples were cleared by centrifuging 20 min at 4°C 3000 ***g***. The supernatant was passed

once through 0.2 μm filters (KC64.1; Roth) to remove debris. Each sample (10 ml in 15 ml Falcon tubes) was incubated for 2.5 h at 4°C under constant end-to-end mixing (approximately 20 rpm) with equilibrated beads corresponding to 20 μl of GFP-trapA (gta100; Proteintech) slurry. After the incubation, beads were washed three times 5 min each with the wash buffer containing 20 mM Tris–HCl pH 7.4, 150 mM NaCl, 0.01% Triton X-100, Plant Protease Inhibitor cocktail (11873580001; Millipore Sigma). Finally, to remove Triton X-100 traces, the beads were washed two additional times 1 min each in the buffer with 20 mM Tris–HCl pH 7.4 and 150 mM NaCl.

Sample preparation and LC-tandem MS data acquisition

Proteins (from GFP-trap enrichment) were submitted to an on-bead digestion. In brief, dry beads were re-dissolved in 25 μl digestion buffer 1 (50 mM Tris, pH 7.5, 2 M urea, 1 mM DTT, 5 ng μl^{-1} trypsin) and incubated for 30 min at 30°C in a Thermomixer with 400 rpm. Next, beads were pelleted, and the supernatant was transferred to a fresh tube. Digestion buffer 2 (50 mM Tris, pH 7.5, 2 M urea, 5 mm 2-chloroacetamide) was added to the beads, after mixing the beads were pelleted, the supernatant was collected and combined with the previous one. The combined supernatants were then incubated o/n at 32°C in a Thermomixer with 400 rpm; samples were protected from light during incubation. The digestion was stopped by adding 1 μl trifluoroacetic acid and desalted with C18 Empore disk membranes according to the StageTip protocol (Rappsilber et al., 2003).

Dried peptides were re-dissolved in 2% acetonitrile (ACN), 0.1% trifluoroacetic acid (10 μl) for analysis and measured without dilution. Samples were analyzed using an EASY-nLC 1000 (Thermo Fisher, Waltham, MA) coupled to a Q Exactive mass spectrometer (Thermo Fisher). Peptides were separated on 16 cm frit-less silica emitters (75 μm inner diameter; New Objective), packed in-house with reversed-phase ReproSil-Pur C18 AQ 1.9 μm resin (Dr. Maisch). Peptides were loaded on the column and eluted for 115 min using a segmented linear gradient of 5–95% solvent B (0 min: 5%B; 0–5 min –>5%B; 5–65 min –>20%B; 65–90 min –>35% B; 90–100 min –>55%; 100–105 min –>95%, 105–115 min –>95%) (solvent A 0% ACN, 0.1% formic acid; solvent B 80% ACN, 0.1% formic acid) at a flow rate of 300 nl min^{-1}. Mass spectra were acquired in data-dependent acquisition mode with a TOP15 method. Mass spectra were acquired in the Orbitrap analyzer with a mass range of 300–1750 *m/z* at a resolution of 70 000 FWHM and a target value of 3×10^6 ions. Precursors were selected with an isolation window of 2.0 *m/z*. HCD fragmentation was performed at a normalized collision energy of 25. Tandem MS spectra were acquired with a target value of 10^5 ions at a resolution of 17 500 FWHM, a maximum injection time (max.) of 55 ms and a fixed first mass of *m/z* 100. Peptides with a charge of +1, >6, or with unassigned charge state were excluded from fragmentation for MS^2, dynamic exclusion for 30 s prevented repeated selection of precursors.

Raw data were processed using MaxQuant software (version 1.6.3.4, http://www.maxquant.org/) (Cox & Mann, 2008) with label-free quantification (LFQ) and iBAQ enabled (Tyanova et al., 2016). Tandem MS spectra were searched by the Andromeda search engine against a combined database containing the sequences from *A. thaliana* (TAIR10_pep_20101214; ftp://ftp.arabidopsis.org/home/tair/Proteins/TAIR10_protein_lists/) and sequences of 248 common contaminant proteins and decoy sequences. Trypsin specificity was required and a maximum of two missed cleavages allowed. Minimal peptide length was set to seven amino acids. Carbamidomethylation of cysteine residues was set as fixed, oxidation of methionine and protein N-terminal acetylation as variable modifications. Peptide-spectrum matches and proteins were retained if they were below a false discovery rate of 1%.

Statistical analysis of the MaxLFQ values was carried out using PERSEUS (version 1.5.8.5; http://www.maxquant.org/). Quantified proteins were filtered for reverse hits and hits "identified by site" and MaxLFQ values were log2 transformed. After grouping samples by condition only those proteins were retained for the subsequent analysis that had three valid values in one of the conditions. Missing values were imputed from a normal distribution (1.8 downshift, separately for each column). Volcano plots were generated in PERSEUS using a false discovery rate of 1% and an S0 = 1.1 The PERSEUS output was exported and further processed using Excel and RStudio.

In silico data analysis and visualization

All data analysis and data representation were performed in RStudio (v. 1.1.463; https://rstudio.com) using the following packages: ggplot2, plyr, multcompView, GGaly, grid, futile.logger, and ggrepel. EDS1-SAG101 crystal structure and EDS1-PAD4 structure model (Wagner et al., 2013) (protein data bank: 4NFU) were visualized using PyMol (2.3.0; https://pymol.org/2/). PAD4 and SAG101 amino acid conservation diagrams in Figure 2 and Figure S1 were generated with WebLogo (https://weblogo.berkeley.edu/logo.cgi) using amino acid sequences published previously (Lapin et al., 2019).

ACKNOWLEDGEMENTS

For this study, the Parker lab was supported by the Max-Planck Society and Deutsche Forschungsgemeinschaft (DFG; German Research Foundation)/Agence Nationale de la Recherche Trilateral "RADAR" grant ANR-15-CE20-0016-01 (JAD and JEP), DFG CRC 680 project B10 (JEP and DL), CRC 670 project TP19 (JEP and DDB), and Germany's Excellence Strategy CEPLAS (EXC-2048/1, Project 390686111) (JEP). The Nakagami lab (HN, SCS, and AH) was supported by the Max Planck Society. MP and LA were each supported by a Mary Beth Baird Scholarship and by the Department of Biological Sciences at the University of North Texas. Open Access funding enabled and organized by Projekt DEAL.

AUTHOR CONTRIBUTIONS

JAD, DDB, and JEP conceived the project; JAD, DDB, EP, DL, SCS, AH, MP, and LA performed experiments; JD, DL, LD, and EP generated biological materials; JAD, SCS, HN, and EP analyzed the data; JD, DDB, and JEP wrote the paper with contributions from JS, HN, DL, SCS, and EP.

CONFLICT OF INTERESTS

The authors declare that they have no competing interests.

DATA AVAILABILITY STATEMENT

The MS data generated in this study are deposited in the PRoteomics IDEntification (PRIDE) database under accession code: PXD029477.

SUPPORTING INFORMATION

Additional Supporting Information may be found in the online version of this article.

Video S1 Video showing spatial orientation of Arabidopsis EDS1-PAD4 cavity residues shown in Figure 1a.

Video S2 Video showing spatial orientation of Arabidopsis EDS1-SAG101 cavity residues shown in Figure 2a.

Table S1 Data sheet containing processed IP-MS data, including iBAQ and LFQ values for YFP-gPAD4 variants, SAG101-YFP variants, and YFP-SH. Table S1 column C provides protein names/AGI codes, column J shows relative normalized protein abundances (LFQ, log_2-scaled) and column L shows negative log_{10} *P* value, shown in Figure 4a and Figure S9b. See Materials and Methods for IP-MS data processing. The mass spectrometry data are deposited at PRIDE database under accession code: PXD029477.

Table S2 List of DNA primers used in this study.

Figure S1. (a) Arabidopsis EDS1-PAD4 heterodimer model (based on Arabidopsis EDS1-SAG101 crystal structure; Wagner *et al*., 2013). EDS1 (black) and PAD4 (gray) with highlighted residues previously mutated in EDS1(as in Figure 1a), (Bhandari et al., 2019; Lapin et al., 2019) and PAD4 residues used here in a PAD4 mutational screen. Left panel shows the PAD4 cavity surface (without EDS1) and the right panel shows the opposite (posterior) side of the EDS1-PAD4 heterodimer. Highlighted residues display carbon atoms in turquoise, oxygen atoms in red and nitrogen atoms in blue. (b–e) Sequence logos indicating the conservation of *At*PAD4 EPD cavity residues shown in (a) in angiosperm and gymnosperm PAD4 protein sequences. Protein sequences were obtained from Lapin et al. (2019). (f) Microscopic immunity phenotypes of 3-week-old Arabidopsis T1 PAD4 EPD cavity mutants as shown in (a) and T3 $PAD4^{WT}$ at 6 dpi with *Hpa* isolate EMWA1 (4×10^4 spores epr ml; recognized by TNL RPP4). Trypan blue-stained leaves showing free hyphae (FH) and hypersensitive cell death (hypersensitive response, HR). Col-0 (resistant) and *pad4-1/sag101-3* (susceptible) functioned as controls. Number of resistant leaves in 12 independent individual lines as indicated. Data pooled from two independent experiments. Black scale bars = 200 μm.

Figure S2. (a) Spatial view of the bottom portion of the Arabidopsis EDS1-PAD4 EPD cavity (based on Arabidopsis EDS1-SAG101 crystal structure (PDB: 4NFU; Wagner et al., 2013), as shown in Figure 1a. EDS1 (black) and PAD4 (gray) with highlighted residues previously mutated in EDS1 (Bhandari et al., 2019; Lapin et al., 2019), and R314 of AtPAD4 analyzed here. Highlighted residues display carbon atoms in turquoise, oxygen atoms in red and nitrogen atoms in blue. (b) Co-immunoprecipitation (GFP-trap) of Arabidopsis YFP-cPAD4 variants, as indicated, with $EDS1^{WT}$-3xFLAG and the non-interacting variants $EDS1^{LLIF}$-3xFLAG transiently co-expressed in *Nicotiana benthamiana* leaves (Wagner et al., 2013). PAD4 variants (PAD4*) retain interaction with $EDS1^{WT}$. EDS1 variant in immunoblot is indicated by EDS1*. A representative image from three independent experiments is shown.

Figure S3. Pathogen growth assay using *Pst avrRps4* (TNL [RPS4/RRS1] ETI) in Arabidopsis independent transgenic and wild-type and mutant control lines as indicated. Four-week-old Arabidopsis plants were syringe-infiltrated with *Pst avrRps4* (OD_{600} = 0.0005) and bacterial titers were determined at 0 dpi (empty squares; *n* = 6) and 3 dpi (filled squares; *n* = 9–12). Symbols of the same color represent two (day 0) or four (day 3) biological replicates in an independent experiment. Bars represent the mean of three experimental replicates ± SE. Letters indicate differences between genotypes as determined by ANOVA (Tukey HSD, $P < 0.01$). (a) As performed in a, using *Pst* DC3000 (basal immunity). (b) TNL (RPP4) ETI assay Arabidopsis independent T3 transgenic lines with wild-type and mutant controls as indicated. Three-week-old Arabidopsis plants were spray-inoculated with *Hpa* EMWA1 (4×10^4 spores per ml) and conidiospores on leaves were quantified at 6 dpi in three independent experiments (squares; *n* = 6). In the box plots, squares of the same color represent two biological replicates in an independent experiment. Letters indicate differences between genotypes as determined by ANOVA (Tukey HSD, $P < 0.05$). (c) PAD4 variant (PAD4*) accumulation in independent stable transgenic Arabidopsis lines expressing YFP-PAD4 as cDNA (*pPAD4:StrepII-YFP-PAD4* constructs) and YFP-gPAD4 as genomic (*pPAD4:YFP-Linker-gPAD4:downstream(ds)PAD4* constructs) variants, as shown in Figure 1 and S3. PAD4 variants were detected by immune-blotting using α-GFP antibody. Samples were harvested at 6 dpi from 3-week-old plants spray-inoculated with *Hpa* EMWA1 (4×10^4 spores per ml). Col-0 and *pad4-1/sag101-3* as controls for antibody specificity. Representative image from three independent experiments.

Figure S4. (a) Subcellular localization of cPAD4 WT and variants in Arabidopsis transgenic T3 lines, as indicated. Similar results were observed in >20 cells per genotype in four biological replicates. White arrowheads = nuclei; scale bar = 50 μm. ChlA, chlorophyll A (autofluorescence); PMT, photon multiplier tube ("bright field"). (b) As in (a), but showing corresponding gPAD4 WT and variant lines.

Figure S5. (a) Microscopic immunity phenotypes of 3-week-old Arabidopsis T1 lines expressing $gPAD4^{R314M}$, $gPAD4^{R314K}$, $gPAD4^{K380R}$, and T3 $gPAD4^{WT}$ at 6 dpi with *Hpa* isolate EMWA1 (4×10^4 spores per ml; recognized by TNL RPP4). Trypan blue-stained leaves showing free hyphae (FH) and hypersensitive cell death (hypersensitive response, HR). Col-0 (resistant) and *pad4-1/sag101-3* (susceptible) were uses as controls. Numbers of resistant leaves in 10–12 independent individual lines are indicated in brackets. Data are representative of three independent experiments, except for $gPAD4^{K380R}$: two independent experiments. Black bars represent 200 μm. (b) PAD4 accumulation in independent transgenic Arabidopsis T1 lines expressing YFP-gPAD4 variants (PAD4*) as in (a). PAD4 variants were detected by immunoblotting using α-GFP antibody. Samples were harvested at 6 dpi from 3-week-old plants spray-inoculated with *Hpa* EMWA1 (4×10^4 spores per ml). Col-0 is a control for antibody specificity. Representative images are from two independent experiments.

Figure S6. Transcript abundance determined by qRT-PCR in 4-week-old Arabidopsis plant lines, as indicated, after syringe infiltration with either buffer (mock, white bars) or *Pst avrRps4* (gray bars; OD_{600} = 0.005) (24 hpi). Data are pooled from three independent experiments, with two to three biological replicates per experiment (*n* = 6–9). Squares of the same color represent biological replicates from an independent experiment. *PAD4*, *EDS1*, *PATHOGENESIS RELATED1 (PR1)*, *AVRPPHB SUSCEPTIBLE 3 (PBS3)*, *ISOCHORISMATE SYNTHASE1 (ICS1)*, and *FLAVIN MONOOXYGENASE1 (FMO1)* transcript abundances were measured relative to *ACTIN2 (ACT2)*. Relative expression is set to Col-0 mock-treated samples. Letters indicate differences between genotypes as determined by ANOVA (Tukey HSD, $P < 0.01$).

Figure S7. (a) Bottom section of the Arabidopsis EDS1-SAG101 EPD cavity (PDB: 4NFU; Wagner *et al*., 2013), as shown in Figure 2a. EDS1 (black) and SAG101 (gray) with highlighted residues previously mutated in EDS1 (Bhandari *et al*., 2019; Lapin *et al*., 2019), and M304 of *At*SAG101 analyzed here. Highlighted residues display carbon atoms in turqoise, oxygen atoms in red, nitrogen atoms in blue and sulfur atoms in yellow. (b) Arabidopsis SAG101 variant (SAG101*) accumulation in independent stable transgenic Arabidopsis lines expressing SAG101-YFP variants as indicated. SAG101 variants were detected by immuno-blotting using α-GFP antibody. Samples were harvested from 4-week-old plants infected with *Pf*0-1 *avrRps4* (OD_{600} = 0.2) at 24 hpi. Col-0 as control for antibody specificity. Representative image from two independent experiments. (c) Subcellular localization of SAG101 variants, as indicated, in Arabidopsis transgenic T3 lines at 6 hpi with

*Pf*0-1 *avrRps4* (OD_{600} = 0.2). Similar results were observed in >20 cells per genotype in four biological replicates. White arrowheads = nuclei; scale bar = 50 μm. ChlA, chlorophyll A (autofluorescence); PMT, photon multiplier tube ("bright field"). (d) Co-immunoprecipitation (GFP-trap) of SAG101-YFP variants, as indicated, with $EDS1^{WT}$-3xFLAG and the non-interacting variant $EDS1^{LLIF}$-3xFLAG transiently co-expressed in *Nicotiana benthamiana* leaves (Wagner *et al.*, 2013). SAG101 variants (SAG101*) retain interaction with $EDS1^{WT}$. EDS1 variant in immunoblot is indicated by EDS1*. A representative image from three independent experiments is shown.

Figure S8. (a) Co-immunoprecipitation (GFP-trap) of *Nb*SAG101b-GFP variants, as indicated, with *Nb*$EDS1a^{WT}$-3xFLAG and YFP transiently co-expressed in *Nb* tobacco leaves (Wagner *et al.*, 2013). *Nb*SAG101b variants (*Nb*SAG101b*) retain interaction with *Nb*EDS1a. A representative image from three independent experiments is shown. (b) Subcellular localization of *Nb*SAG101b variants, as indicated, accumulation in *Nb* tobacco leaves at 2 days after transient expression of *Nb*SAG101b-GFP variants. Similar results were observed in >20 cells per genotype in three biological replicates. White arrowheads = nuclei; scale bar = 50 μm. ChlA, chlorophyll A (autofluorescence); PMT, photon multiplier tube ("bright field"). (c) *b*SAG101b variant (*Nb*SAG101b*), YFP and XopQ accumulation in *Nb* tobacco leaves at 2 days after transient expression of *Nb*SAG101-GFP variants, YFP, and/ XopQ-MYC as shown in Figure 3a. *Nb*SAG101b-GFP variants and YFP and XopQ-MYC were detected by immuno-blotting using α-GFP and α-MYC antibody, respectively. Representative image from four independent experiments shown in Figure 3a. (d) *Nb*SAG101b and YFP accumulation during *Xcv* infection in *Nb* tobacco leaves 2 days after transient expression of *Nb*SAG101-GFP variants and YFP as shown in Figure 3b. *Nb*SAG101b-GFP variants and YFP were detected by immunoblotting using α-GFP. Representative image from four independent experiments shown in Figure 3b.

Figure S9. (a) PAD4, YFP, and SAG101 accumulation in independent stable transgenic Arabidopsis lines expressing YFP-gPAD4 variants, SAG101-YFP variants and YFP-SH. PAD4 variants, SAG101 variants and YFP-SH were detected by immunoblotting using α-GFP antibody. Input samples for IP-MS analysis in Figure 4. (b) Volcano plots of normalized abundances (LFQ, $\log_2$ scale) for proteins co-purified with YFP-$gPAD4^{WT}$versus YFP-$gPAD4^{R314A}$ (left) and $SAG101^{WT}$-YFP versus $SAG101^{M304R}$-YFP (right) Proteins significantly enriched relative to PAD4 and SAG101 mutant variant are shown in orange in the top right corner of each plot. As a cut-off for significant interactions we used the following threshold: protein was detected in three of four experiments; $|\log_2$ (WT protein IP/mutant protein IP)$| \geq 1$, $P \leq 0.05$. Missing values were imputed.

Figure S10. Transcript abundances determined by qRT-PCR in samples harvested during IP-MS experiments shown in Figure 4. Data are from one biological replicate from four independent experiments per time point ($n = 4$). Squares of the same color represent biological replicates from an independent experiment. *PBS3*, *ICS1*, *FMO1*, *CRK36*, *ADR1-L1*, *NRG1.1*, *RPP8* and *RPP1* transcript abundances were measured relative to *ACTIN2 (ACT2)*. Relative expression is set to Col-0 mock-treated samples. Letters indicate differences between genotypes as determined by ANOVA (Tukey HSD; $P < 0.01$).

REFERENCES

Adlung, N., Prochaska, H., Thieme, S., Banik, A., Blueher, D., John, P. et al. (2016) Non-host resistance induced by the Xanthomonas effector XopQ is widespread within the genus Nicotiana and functionally depends on EDS1. *Frontiers in Plant Science*, **7**, 1796.

Albert, I., Hua, C.L., Nurnberger, T., Pruitt, R.N. & Zhang, L.S. (2020) Surface sensor systems in plant immunity. *Plant Physiology*, **182**, 1582–1596.

Barragan, C.A., Wu, R., Kim, S.T., Xi, W.Y., Habring, A., Hagmann, J. et al. (2019) RPW8/HR repeats control NLR activation in *Arabidopsis thaliana*. *PLoS Genetics*, **15**, e1008313.

Bayless, A.M. & Nishimura, M.T. (2020) Enzymatic functions for toll/interleukin-1 receptor domain proteins in the plant immune system. *Frontiers in Genetics*, **11**, 539.

Bensmihen, S., To, A., Lambert, G., Kroj, T., Giraudat, J. & Parcy, F. (2004) Analysis of an activated ABI5 allele using a new selection method for transgenic Arabidopsis seeds. *FEBS Letters*, **561**, 127–131.

Berkey, R., Zhang, Y., Ma, X., King, H., Zhang, Q., Wang, W. *et al.* (2017) Homologues of the RPW8 resistance protein are localized to the extrahaustorial membrane that is likely synthesized de novo. *Plant Physiology*, **173**, 600–613.

Bhandari, D.D., Lapin, D., Kracher, B., von Born, P., Bautor, J., Niefind, K. *et al.* (2019) An EDS1 heterodimer signalling surface enforces timely reprogramming of immunity genes in Arabidopsis. *Nature Communications*, **10**, 772.

Bhattacharjee, S., Halane, M.K., Kim, S.H. & Gassmann, W. (2011) Pathogen effectors target Arabidopsis EDS1 and alter its interactions with immune regulators. *Science*, **334**, 1405–1408.

Bi, G., Su, M., Li, N., Liang, Y., Dang, S., Xu, J. *et al.* (2021) The ZAR1 resistosome is a calcium-permeable channel triggering plant immune signaling. *Cell*, **184**, 3528–3541.e3512.

Bonardi, V., Tang, S.J., Stallmann, A., Roberts, M., Cherkis, K. & Dangl, J.L. (2011) Expanded functions for a family of plant intracellular immune receptors beyond specific recognition of pathogen effectors. *Proceedings of the National Academy of Sciences of the United States of America*, **108**, 16463–16468.

Castel, B., Ngou, P.M., Cevik, V., Redkar, A., Kim, D.S., Yang, Y. *et al.* (2019) Diverse NLR immune receptors activate defence via the RPW8-NLR NRG1. *New Phytologist*, **222**, 966–980.

Castel, B., Wu, Y., Xiao, S. & Jones, J.D.G. (2019) An rpw8 quadruple mutant of Arabidopsis Col-0 is partially compromised in bacterial and fungal resistance. *bioRxiv*, 839308. https://doi.org/10.1101/839308

Chae, E., Bomblies, K., Kim, S.T., Karelina, D., Zaidem, M., Ossowski, S. *et al.* (2014) Species-wide genetic incompatibility analysis identifies immune genes as hot spots of deleterious epistasis. *Cell*, **159**, 1341–1351.

Couto, D. & Zipfel, C. (2016) Regulation of pattern recognition receptor signalling in plants. *Nature Reviews Immunology*, **16**, 537–552.

Cox, J. & Mann, M. (2008) MaxQuant enables high peptide identification rates, individualized p.p.b.-range mass accuracies and proteome-wide protein quantification. *Nature Biotechnology*, **26**, 1367–1372.

Cui, H., Gobbato, E., Kracher, B., Qiu, J., Bautor, J. & Parker, J.E. (2017) A core function of EDS1 with PAD4 is to protect the salicylic acid defense sector in Arabidopsis immunity. *The New Phytologist*, **213**, 1802–1817.

Cui, H., Qiu, J., Zhou, Y., Bhandari, D.D., Zhao, C., Bautor, J. *et al.* (2018) Antagonism of Transcription Factor MYC2 by EDS1/PAD4 Complexes Bolsters Salicylic Acid Defense in Arabidopsis Effector-Triggered Immunity. *Molecular Plant*, **11**, 1053–1066.

Cui, H.T., Tsuda, K. & Parker, J.E. (2015) Effector-triggered immunity: from pathogen perception to robust defense. *Annual Review of Plant Biology*, **66**, 487–511.

Daskalov, A., Habenstein, B., Sabate, R., Berbon, M., Martinez, D., Chaignepain, S. *et al.* (2016) Identification of a novel cell death-inducing domain reveals that fungal amyloid-controlled programmed cell death is related to necroptosis. *Proceedings of the National Academy of Sciences of the United States of America*, **113**, 2720–2725.

Dongus, J.A., Bhandari, D.D., Patel, M., Archer, L., Dijkgraaf, L., Deslandes, L. *et al.* (2020) The Arabidopsis PAD4 lipase-like domain is sufficient for resistance to green peach aphid. *Molecular Plant-Microbe Interactions: MPMI*, **33**, 328–335.

Dongus, J.A. & Parker, J.E. (2021) EDS1 signalling: at the nexus of intracellular and surface receptor immunity. *Current Opinion in Plant Biology*, **62**, 102039.

Feehan, J.M., Castel, B., Bentham, A.R. & Jones, J.D.G. (2020) Plant NLRs get by with a little help from their friends. *Current Opinion in Plant Biology*, **56**, 99–108.

Gantner, J., Ordon, J., Kretschmer, C., Guerois, R. & Stuttmann, J. (2019) An EDS1-SAG101 complex is essential for TNL-mediated immunity in *Nicotiana benthamiana*. *Plant Cell*, **31**, 2456–2474.

Garcia, A.V., Blanvillain-Baufume, S., Huibers, R.P., Wiermer, M., Li, G., Gobbato, E. *et al.* (2010) Balanced nuclear and cytoplasmic activities of

EDS1 are required for a complete plant innate immune response. *PLoS Pathogens*, **6**, e1000970.

Heidrich, K., Wirthmueller, L., Tasset, C., Pouzet, C., Deslandes, L. & Parker, J.E. (2011) Arabidopsis EDS1 connects pathogen effector recognition to cell compartment-specific immune responses. *Science*, **334**, 1401–1404.

Hinsch, M. & Staskawicz, B. (1996) Identification of a new Arabidopsis disease resistance locus, RPs4, and cloning of the corresponding avirulence gene, avrRps4, from *Pseudomonas syringae* pv. pisi. *Molecular Plant-Microbe Interactions: MPMI*, **9**, 55–61.

Horsefield, S., Burdett, H., Zhang, X.X., Manik, M.K., Shi, Y., Chen, J. *et al.* (2019) NAD(+) cleavage activity by animal an plant TIR domains in cell death pathways. *Science*, **365**, 793–+.

Huh, S.U., Cevik, V., Ding, P.T., Duxbury, Z., Ma, Y., Tomlinson, L. *et al.* (2017) Protein-protein interactions in the RPS4/RRS1 immune receptor complex. *PLoS Pathogens*, **13**, e1006376.

Jacob, P., Kim, N.H., Wu, F., El-Kasmi, F., Chi, Y., Walton, W.G. *et al.* (2021) Plant "helper" immune receptors are Ca(2+)-permeable nonselective cation channels. *Science*, **373**, 420–425.

Jang, S., Torti, S. & Coupland, G. (2009) Genetic and spatial interactions between FT, TSF and SVP during the early stages of floral induction in Arabidopsis. *The Plant Journal*, **60**, 614–625.

Jones, J.D. & Dangl, J.L. (2006) The plant immune system. *Nature*, **444**, 323–329.

Ke, Y.G., Kang, Y.R., Wu, M.X., Liu, H.B., Hui, S.G., Zhang, Q.L. *et al.* (2019) Jasmonic acid-involved OsEDS1 signaling in rice-bacteria interactions. *Rice*, **12**, 25.

Kim, T.H., Kunz, H.H., Bhattacharjee, S., Hauser, F., Park, J., Engineer, C. *et al.* (2012) Natural variation in small molecule-induced TIR-NB-LRR signaling induces root growth arrest via EDS1- and PAD4-complexed R protein VICTR in Arabidopsis. *Plant Cell*, **24**, 5177–5192.

Klock, H.E. & Lesley, S.A. (2009) The Polymerase Incomplete Primer Extension (PIPE) method applied to high-throughput cloning and site-directed mutagenesis. *Methods in Molecular Biology*, **498**, 91–103.

Koch, E. & Slusarenko, A. (1990) Arabidopsis is susceptible to infection by a downy mildew fungus. *Plant Cell*, **2**, 437–445.

Lapin, D., Bhandari, D.D. & Parker, J.E. (2020) Origins and immunity networking functions of EDS1 family proteins. *Annual Review of Phytopathology*, **58**, 253–276.

Lapin, D., Johanndrees, O., Wu, Z., Li, X. & Parker, J.E. (2022) Molecular innovations in plant TIR-based immunity signaling. *The Plant Cell*, koac035.

Lapin, D., Kovacova, V., Sun, X., Dongus, J.A., Bhandari, D., von Born, P. *et al.* (2019) A coevolved EDS1-SAG101-NRG1 module mediates cell death signaling by TIR-domain immune receptors. *Plant Cell*, **31**, 2430–2455.

Le Roux, C., Huet, G., Jauneau, A., Camborde, L., Tremousaygue, D., Kraut, A. *et al.* (2015) A receptor pair with an integrated decoy converts pathogen disabling of transcription factors to immunity. *Cell*, **161**, 1074–1088.

Li, L., Habring, A., Wang, K. & Weigel, D. (2020) Atypical resistance protein RPW8/HR triggers oligomerization of the NLR immune receptor RPP7 and autoimmunity. *Cell Host & Microbe*, **27**, 405.

Logemann, E., Birkenbihl, R.P., Uelker, B. & Somssich, I.E. (2006) An improved method for preparing Agrobacterium cells that simplifies the Arabidopsis transformation protocol. *Plant Methods*, **2**, 16.

Louis, J., Gobbato, E., Mondal, H.A., Feys, B.J., Parker, J.E. & Shah, J. (2012) Discrimination of Arabidopsis PAD4 activities in defense against green peach aphid and pathogens. *Plant Physiology*, **158**, 1860–1872.

Louis, J. & Shah, J. (2015) Plant defence against aphids: the PAD4 signalling nexus. *Journal of Experimental Botany*, **66**, 449–454.

Ma, S., Lapin, D., Liu, L., Sun, Y., Song, W., Zhang, X. *et al.* (2020) Direct pathogen-induced assembly of an NLR immune receptor complex to form a holoenzyme. *Science*, **370**, eabe3069.

Mahdi, L.K., Huang, M., Zhang, X., Nakano, R.T., Kopp, L.B., Saur, I.M.L. *et al.* (2020) Discovery of a family of mixed lineage kinase domain-like proteins in plants and their role in innate immune signaling. *Cell Host & Microbe*, **28**, 813–824.e6.

Martin, R., Qi, T., Zhang, H., Liu, F., King, M., Toth, C. *et al.* (2020) Structure of the activated ROQ1 resistosome directly recognizing the pathogen effector XopQ. *Science*, **370**, eabd9993.

Mindrebo, J.T., Nartey, C.M., Seto, Y., Burkart, M.D. & Noel, J.P. (2016) Unveiling the functional diversity of the alpha/beta hydrolase superfamily in the plant kingdom. *Current Opinion in Structural Biology*, **41**, 233–246.

Mine, A., Nobori, T., Salazar-Rondon, M.C., Winkelmuller, T.M., Anver, S., Becker, D. *et al.* (2017) An incoherent feed-forward loop mediates robustness and tunability in a plant immune network. *EMBO Reports*, **18**, 464–476.

Monteiro, F. & Nishimura, M.T. (2018) Structural, functional, and genomic diversity of plant NLR proteins: an evolved resource for rational engineering of plant immunity. *Annual Review of Phytopathology*, **56**, 243–267.

Muskett, P.R., Kahn, K., Austin, M.J., Moisan, L.J., Sadanandom, A., Shirasu, K. *et al.* (2002) Arabidopsis RAR1 exerts rate-limiting control of R gene-mediated defenses against multiple pathogens. *Plant Cell*, **14**, 979–992.

Nalam, V., Louis, J., Patel, M. & Shah, J. (2018) Arabidopsis-green peach aphid interaction: rearing the insect, no-choice and fecundity assays, and electrical penetration graph technique to study insect feeding behavior. *Bio-Protocol*, **8**, e2950.

Neubauer, M., Serrano, I., Rodibaugh, N., Bhandari, D.D., Bautor, J., Parker, J.E. *et al.* (2020) Arabidopsis EDR1 protein kinase regulates the association of EDS1 and PAD4 to inhibit cell death. *Molecular Plant-Microbe Interactions*, **33**, 693–703.

Ngou, B.P.M., Ahn, H.K., Ding, P. & Jones, J.D.G. (2021) Mutual potentiation of plant immunity by cell-surface and intracellular receptors. *Nature*, **592**, 110–115.

Parker, J.E., Hessler, G. & Cui, H. (2021) A new biochemistry connecting pathogen detection to induced defense in plants. *The New phytologist.*, **234**, 819–826.

Pegadaraju, V., Louis, J., Singh, V., Reese, J.C., Bautor, J., Feys, B.J. *et al.* (2007) Phloem-based resistance to green peach aphid is controlled by Arabidopsis PHYTOALEXIN DEFICIENT4 without its signaling partner ENHANCED DISEASE SUSCEPTIBILITY1. *The Plant Journal*, **52**, 332–341.

Petrie, E.J., Czabotar, P.E. & Murphy, J.M. (2019) The structural basis of necroptotic cell death signaling. *Trends in Biochemical Sciences*, **44**, 53–63.

Pruitt, R.N., Locci, F., Wanke, F., Zhang, L., Saile, S.C., Joe, A. *et al.* (2021) The EDS1-PAD4-ADR1 node mediates Arabidopsis pattern-triggered immunity. *Nature*, **598**, 495–499.

Rappsilber, J., Ishihama, Y. & Mann, M. (2003) Stop and go extraction tips for matrix-assisted laser desorption/ionization, nanoelectrospray, and LC/MS sample pretreatment in proteomics. *Analytical Chemistry*, **75**, 663–670.

Rietz, S., Stamm, A., Malonek, S., Wagner, S., Becker, D., Medina-Escobar, N. *et al.* (2011) Different roles of enhanced disease susceptibility1 (EDS1) bound to and dissociated from Phytoalexin Deficient4 (PAD4) in Arabidopsis immunity. *The New Phytologist*, **191**, 107–119.

Saile, S.C., Jacob, P., Castel, B., Jubic, L.M., Salas-Gonzales, I., Backer, M. *et al.* (2020) Two unequally redundant "helper" immune receptor families mediate *Arabidopsis thaliana* intracellular "sensor" immune receptor functions. *PLoS Biology*, **18**, e3000783.

Schultink, A., Qi, T., Lee, A., Steinbrenner, A.D. & Staskawicz, B. (2017) Roq1 mediates recognition of the Xanthomonas and Pseudomonas effector proteins XopQ and HopQ1. *The Plant Journal*, **92**, 787–795.

Sun, X., Lapin, D., Feehan, J.M., Stolze, S.C., Kramer, K., Dongus, J.A. *et al.* (2021) Pathogen effector recognition-dependent association of NRG1 with EDS1 and SAG101 in TNL receptor immunity. *Nature Communications*, **12**, 3335.

Thieme, F., Koebnik, R., Bekel, T., Berger, C., Boch, J., Buettner, D. *et al.* (2005) Insights into genome plasticity and pathogenicity of the plant pathogenic bacterium *Xanthomonas campestris* pv. vesicatoria revealed by the complete genome sequence. *Journal of Bacteriology*, **187**, 7254–7266.

Thomas, W.J., Thireault, C.A., Kimbrel, J.A. & Chang, J.H. (2009) Recombineering and stable integration of the *Pseudomonas syringae* pv. *syringae* 61 hrp/hrc cluster into the genome of the soil bacterium *Pseudomonas fluorescens* Pf0-1. *The Plant Journal*, **60**, 919–928.

Tian, H., Wu, Z., Chen, S., Ao, K., Huang, W., Yaghmaiean, H. *et al.* (2021) Activation of TIR signalling boosts pattern-triggered immunity. *Nature*, **598**, 500–503.

Tyanova, S., Temu, T. & Cox, J. (2016) The MaxQuant computational platform for mass spectrometry-based shotgun proteomics. *Nature Protocols*, **11**, 2301–2319.

Voss, M., Toelzer, C., Bhandari, D.D., Parker, J.E. & Niefind, K. (2019) Arabidopsis immunity regulator EDS1 in a PAD4/SAG101-unbound form is a monomer with an inherently inactive conformation. *Journal of Structural Biology*, **208**, 107390.

Wagner, S., Stuttmann, J., Rietz, S., Guerois, R., Brunstein, E., Bautor, J. *et al.* (2013) Structural basis for signaling by exclusive EDS1 heteromeric complexes with SAG101 or PAD4 in plant innate immunity. *Cell Host & Microbe*, **14**, 619–630.

Wan, L., Essuman, K., Anderson, R.G., Sasaki, Y., Monteiro, F., Chung, E.H. *et al.* (2019) TIR domains of plant immune receptors are NAD(+)-cleaving enzymes that promote cell death. *Science*, **365**, 799-+.

Wan, W.L., Frohlich, K., Pruitt, R.N., Nurnberger, T. & Zhang, L.S. (2019) Plant cell surface immune receptor complex signaling. *Current Opinion in Plant Biology*, **50**, 18–28.

Wang, J., Wang, J., Hu, M., Wu, S., Qi, J., Wang, G. *et al.* (2019) Ligand-triggered allosteric ADP release primes a plant NLR complex. *Science*, **364**, eaav5868.

Wang, J.Z., Hu, M.J., Wang, J., Qi, J.F., Han, Z.F., Wang, G.X. *et al.* (2019) Reconstitution and structure of a plant NLR resistosome conferring immunity. *Science*, **364**, eaav5870.

Wang, L., Dong, M., Zhang, Q., Wu, Y., Hu, L., Parson, J.F. *et al.* (2020) Silicon modulates multi-layered defense against powdery mildew in Arabidopsis. *Phytopathology Research*, **2**, 7.

Wang, W., Wen, Y., Berkey, R. & Xiao, S. (2009) Specific targeting of the Arabidopsis resistance protein RPW8.2 to the interfacial membrane encasing the fungal Haustorium renders broad-spectrum resistance to powdery mildew. *Plant Cell*, **21**, 2898–2913.

Wiermer, M., Feys, B.J. & Parker, J.E. (2005) Plant immunity: the EDS1 regulatory node. *Current Opinion in Plant Biology*, **8**, 383–389.

Witte, C.P., Noël, L.D., Gielbert, J., Parker, J.E. & Romeis, T. (2004) Rapid one-step protein purification from plant material using the eight-amino acid StrepII epitope. *Plant Molecular Biology*, **55**, 135–147.

Wroblewski, T., Spiridon, L., Martin, E.C., Petrescu, A.J., Cavanaugh, K., Truco, M.J.P. *et al.* (2018) Genome-wide functional analyses of plant coiled-coil NLR-type pathogen receptors reveal essential roles of their N-terminal domain in oligomerization, networking, and immunity. *PLoS Biology*, **16**, e2005821.

Wu, C.H., Abd-El-Haliem, A., Bozkurt, T.O., Belhaj, K., Terauchi, R., Vossen, J.H. *et al.* (2017) NLR network mediates immunity to diverse plant pathogens. *Proceedings of the National Academy of Sciences of the United States of America*, **114**, 8113–8118.

Wu, Z., Tian, L., Liu, X., Huang, W., Zhang, Y. & Li, X. (2021) The N-terminally truncated helper NLR NRG1C antagonizes immunity mediated by its full-length neighbors NRG1A and NRG1B. *The Plant Cell*, koab285.

Wu, Z., Tian, L., Liu, X., Zhang, Y. & Li, X. (2022) TIR signaling promotes the interactions between EDS1/PAD4 and ADR1-L1 and oligomerization of ADR1-L1. *Plant Pysiology*, **187**, 681–686.

Wu, Z.S., Li, M., Dong, O.X., Xia, S.T., Liang, W.W., Bao, Y.K. *et al.* (2019) Differential regulation of TNL-mediated immune signaling by redundant helper CNLs. *New Phytologist*, **222**, 938–953.

Xiao, S., Brown, S., Patrick, E., Brearley, C. & Turner, J.G. (2003) Enhanced transcription of the Arabidopsis disease resistance genes RPW8.1 and RPW8.2 via a salicylic acid-dependent amplification circuit is required for hypersensitive cell death. *Plant Cell*, **15**, 33–45.

Xiao, S., Calis, O., Patrick, E., Zhang, G., Charoenwattana, P., Muskett, P. *et al.* (2005) The atypical resistance gene, RPW8, recruits components of basal defence for powdery mildew resistance in Arabidopsis. *The Plant Journal*, **42**, 95–110.

Xiao, S., Ellwood, S., Calis, O., Patrick, E., Li, T., Coleman, M. *et al.* (2001) Broad-spectrum mildew resistance in *Arabidopsis thaliana* mediated by RPW8. *Science*, **291**, 118–120.

Xiao, S., Emerson, B., Ratanasut, K., Patrick, E., O'Neill, C., Bancroft, I. *et al.* (2004) Origin and maintenance of a broad-spectrum disease resistance locus in Arabidopsis. *Molecular Biology and Evolution*, **21**, 1661–1672.

Yu, D., Song, W., Tan, E.Y.J., Liu, L., Cao, Y., Jirschitzka, J. *et al.* (2021) TIR domains of plant immune receptors are 2′,3′-cAMP/cGMP synthetases mediating cell death. *bioRxiv*, 2021.2011.2009.467869.

Yuan, M., Jiang, Z., Bi, G., Nomura, K., Liu, M., He, S.Y. *et al.* (2021) Pattern-recognition receptors are required for NLR-mediated plant immunity. *Nature*, **592**, 105–109.

Zavaliev, R., Mohan, R., Chen, T. & Dong, X. (2020) Formation of NPR1 condensates promotes cell survival during the plant immune response. *Cell*, **182**, 1093–1108.e1018.

Zhang, Y.L., Song, G.Y., Lai, N.K., Nagalakshmi, U., Li, Y.Y., Zheng, W.J. *et al.* (2019) TurboID-based proximity labeling reveals that UBR7 is a regulator of N NLR immune receptor-mediated immunity. *Nature Communications*, **10**, 3252.